Source Term Analysis of FeCrAl Accident Tolerant Fuel using MELCOR

Una Baker[a], Yong-Joon Choi[b], Nicholas Rollins[c], Khang Nguyen[c], WooHyun Jung[a], Abe Whitmeyer[a], Jason Hou[c] and Ben Lindley[a*]

[a]*Reactor Technology Integration Group, Department of Nuclear Engineering and Engineering Physics, Madison, WI, 53711*

b Idaho National Laboratory

c Department of Nuclear Engineering, North Carolina State University, Raleigh, NC 27695

Abstract

It has been established that incremental improvements in beyond design basis accident performance can be achieved through accident tolerant fuel (ATF). However, they have the potential to recover margin with respect to conventional fuel and therefore enhance plant economics through uprate or cycle length increase. To realize this potential, it is necessary to quantify the reduction in source term due to use of ATF, and correspondingly how this is affected by increasing the cycle length and/or burnup. This requires development of a risk informed analysis methodology for ATF under high burnup conditions, which is being developed within LWRS. To this end, a MELCOR simulation of FeCrAl ATF in a recovered Large Break LOCA (LBLOCA) scenario has been developed, using a model based on the Zion Pressurized Water Reactor (PWR). The new user defined material capability, along with the inclusion of detailed neutronics- and depletion-derived parameters such as core power distribution, decay heat behavior, and fission product inventories, allows a more detailed simulation of FeCrAl clad material properties and behavior than has previously been possible using MELCOR. These detailed FeCrAl results were compared with a zircaloy clad model to investigate the differences between the two clad types and quantify the benefits of FeCrAl ATF with an 18-month cycle. Next, the fuel cycle with ATF was extended to 24 months, to determine whether any additional safety margin provided by FeCrAl ATF could be leveraged to implement high burnup FeCrAl-clad fuel while retaining the same operating and safety limits as current zircaloy-clad fuel. For the particular scenario analyzed, the delay to fuel failure from using ATF was of the same order as the LOCA recovery time, and hence significant in reducing fission product release, with the 24-month FeCrAl core performing better than the 18-month zircaloy core. It is noted that for other transients, the reduction in release due to using FeCrAl may be less significant. The material model developed here can be used in such further studies in support of determining the overall source term.

Keywords: MELCOR, FeCrAl, Accident Tolerant Fuel, LOCA

*Corresponding author: lindley2@wisc.edu

Nomenclature

18m	18 month (Cycle Length)
24m	24 month (Cycle Length)
ATF	Accident Tolerant Fuel
BDBA	Beyond Design Basis Accident
ECCS	Emergency Core Cooling System
EO(E)C	End Of (Equilibrium) Cycle
GUI	Graphical User Interface
INL	Idaho National Laboratories
LBLOCA	Large Break Loss Of Coolant Accident
LOCA	Loss Of Coolant Accident
LPSI	Low Pressure Safety Injection system
LWR	Light Water Reactor
LWRS	Light Water Reactor Sustainability
NRC	Nuclear Regulatory Commission
ORNL	Oak Ridge National Laboratory
PNNL	Pacific Northwest National Laboratory
PWR	Pressurized Water Reactor
SNL	Sandia National Laboratories
UDGC	User-Defined General Coating
UDM	User-Defined Material
Zry	Zircaloy

1 Introduction

The U.S. Department of Energy Light Water Reactor Sustainability (LWRS) Program is promoting a wide range of research and development activities with the goal to maximize both the safety and economically efficient performance of NPPs through improved scientific understanding, especially given that many plants are considering second license renewal. Safety can be achieved more economically by using a risk-informed ecosystem with deployment of methodologies and technologies that enable better representation of safety margins and the factors that contribute to cost and safety, such as that being developed by the Risk-Informed Systems Analysis (RISA) Pathway within the LWRS program.

Accident Tolerant Fuel (ATF) has been proposed as a safety enhancement which can be implemented in current reactors, that have the potential to provide additional coping time [1], [2] and therefore recover safety margin [3]. Within a risk-informed ecosystem, this potentially provides an opportunity to increase performance, e.g., core power or cycle length, by utilizing the recovered margin. Additionally, current efforts to commercialize fuels of enrichment higher than 5% (LEU+) facilitate such uprates or cycle length increases while maintaining fuel burnup at competitive levels and offsetting any neutronic penalty from the ATF [4].

A fuel is defined as having improved accident tolerance if it is more resilient to a loss of core cooling capability while also maintaining or increasing fuel performance during normal operation, when compared to the standard UO_2-Zry fuel [5]. The ideal characteristics for ATF clad are slower reaction kinetics with steam, a slower rate of hydrogen production or improved clad properties. For the pellet, improved fuel properties and/or an enhanced capacity to retain fission products [6] are desirable. As a key benefit of ATF is its ability to integrate into current reactor systems, the designs should also be compatible with existing fuel assembly geometries, fuel cycles, and plant operations.

Some examples of ATF candidates are a fully ceramic micro-encapsulated fuel in a silicon carbide (SiC) matrix which can withstand significantly higher temperatures than current fuels [7], [8]; and the iron-chromium-aluminum alloy FeCrAl, which exhibits lower oxidation kinetics and reduced hydrogen production compared with Zry clad [9], [10].

Significant work has been performed using individual fuel performance calculations using a dedicated fuel behavior code such as FRAPTRAN or BISON [11], [12], [13]. FRAPTRAN is designed to perform transient fuel rod thermal and mechanical calculations and has recently been extended to enable ATF simulation. Recent developments include definition of creep coefficients to model ATF clad burst characteristics [14]; the addition of a multi-layer model to account for the different deformation behavior of ATF [15]; and the combination of FRAPTRAN with FRAPCON to create FRAP-ATF [16]. FRAPTRAN-2.0 was also recently extended to modelling of FeCrAl [17]. Recent work using the BISON finite element-based fuel performance code includes an investigation into FeCrAl clad behavior and mechanical failure under normal and accident conditions [18], [19]; an examination of fuel performance and accident scenarios using chromium-coated Zry clad [20], [21]; and improvement of modelling capabilities for doped fuel types such as U_3Si_2 or Cr_2O_3 [22]. BISON is also integrated into the MOOSE framework developed by Idaho National Laboratory (INL) [23], [24], allowing the fuel performance results to be considered as part of a larger-scale multiphysics simulation.

To enable such operational benefits to be achieved, the source term with ATF must be quantified in the uprate or higher burnup condition. This requires source term analysis utilizing representative ATF material models and incorporating the additional fission product inventory of higher burnup fuels. This requires analysis of beyond design basis accident (BDBA) scenarios.

A useful simulation of ATF in a BDBA scenario requires the capability to solve complex interactions between neutronics, thermal hydraulics, and thermo-mechanics on scales ranging from the subatomic to the environmental. Such a multi-scale simulation presents a challenge in its own right, even before the additional complications of non-standard fuel and clad materials are introduced. This can be performed in systems codes such as MELCOR. MELCOR is an integrated engineering-level code developed by Sandia National Laboratories (SNL) for the US Nuclear Regulatory Committee (NRC) and designed to model a broad spectrum of severe accident phenomena in Light Water Reactors (LWRs) and non-LWRs [25], [26]. Although MELCOR does not explicitly model neutronics interactions, its sophisticated systems approach allows the simulation of a wide range of severe accident phenomena. These include thermal-hydraulic effects in the reactor core, cavity, and containment; the process of core uncovering and subsequent fuel pellet chemical interactions; melting and relocation of core materials and failure of the lower vessel head; and the generation and behavior of hydrogen and aerosols. MELCOR also has a dedicated accident analysis code, MACCS, which models the impact of a nuclear accident on the surrounding environment [27]. MACCS has been used by the US NRC for probabilistic

risk assessment (PRA) of nuclear facilities, sensitivity studies to identify important contributors to PRA, and cost-benefit analysis to find suitable preventative measures. This additional capability extends the ATF analysis possible with MELCOR and motivates the decision to use MELCOR for this work.

Previous work using MELCOR to model ATF has progressed as the code capabilities have evolved. Older versions of MELCOR placed limitations on which materials could be considered in the core, restricting simulations to using a selection of default materials including Zr and ZrO_2 but not including FeCrAl. Research performed using this code version often redefined the properties of the default Zr materials to force them to behave like FeCrAl, in an approximation which nevertheless provided a basis for comparison of the two materials [28], [29], [30], [31]. In further work INL extended the MELCOR capabilities by adding models for SiC and FeCrAl along with their oxides, as well as the ability to model a coating to the clad which could be defined separately, the User Defined General Coating (UDGC) model [32] [33] [34].

The UDGC model has been successfully used to model ATF in LWR severe accident scenarios such as mitigated and unmitigated station blackouts and a simulation of the Three Mile Island accident [29], [30], [35], [36], [37], [38]. With the latest release of MELCOR 2.2, the UDGC model has been integrated into the MELCOR source code and extended to provide additional clad oxidation capabilities as a new User-Defined Material (UDM) model [39], [40]. This UDM model has been employed for severe accident analysis of FeCrAl ATF in a long-term station blackout incident for a BWR and to model hydrogen production in a FeCrAl simulation recreating the PHEBUS experiments [41], [42].

As the MELCOR UDM method is still relatively new, at present only limited literature exists using this model for ATF modelling. The FeCrAl alloy 'Ironclad' C26M is also a comparatively recent development and studies using this material in MELCOR simulations are limited [43]. The detailed model description and MELCOR methodology described here aim to supplement the existing literature with a C26M example case study which may be useful for future research modelling C26M ATF using MELCOR.

In this paper, we focus specifically on increased burnup fuels, and use of FeCrAl as an ATF clad. We develop a new state-of-the-art model of FeCrAl in MELCOR 2.2, the latest version of the code, using its user defined material (UDM) capability. We then use this model to investigate the impact of FeCrAl clad on core performance during a recovered large break loss of coolant accident (LBLOCA). The impact of moving to a 24-month cycle with high burnup (HBU) fuel on core damage, hydrogen generation and fission product release is also investigated. In particular, the latter supports quantification of the source term with FeCrAl clad, an area with relatively limited data in the open literature. Finally, the detailed model description and MELCOR methodology described here provide a basis for future research on source term analysis of proposed FeCrAl clads.

1.1 FeCrAl Clad

FeCrAl alloys usually contain 12 – 21% Cr and 4 – 6% Al, with other elements such as molybdenum (Mo), yttrium (Y), zirconium (Zr), hafnium (Hf), and titanium (Ti) sometimes present in small amounts [44]. Most FeCrAl alloys fall neatly into two groups: high-Cr FeCrAl and low-Cr FeCrAl. FeCrAl with higher Cr content exhibits better oxidation resistance at higher temperatures, while a lower Cr content produces a lower neutronic impact due to fewer parasitic absorptions in the reactor core [45], [46]. The compositions of three of the most popular FeCrAl alloys are listed in Table 1.

Table 1: FeCrAl alloy compositions (mass percent, Fe balance)

Alloy	Fe	Cr	Al	Mo	Other
Kanthal APMT [47]	bal.	21.0	5.0	3.0	-
'Ironclad' C26M [48]	bal.	12.0	6.0	2.0	0.2 Si + 0.03 Y
FeCrAl ODS [10]	bal.	12.0	6.0	-	0.5 Ti + Zr + Y_2O_3 + Fe_2O_3

The main benefit of FeCrAl as an ATF clad is its superior high-temperature oxidation resistance compared to Zry. This arises due to the Cr in the material, which has been observed to preferentially oxidize before the other alloy elements at operating temperatures to naturally form a protective Cr_2O_3 oxide coating [49]. This prevents the rest of the clad from oxidizing, resulting in less heat being generated and less deterioration of the fuel pellet. At elevated temperatures (up to about 1350°C), oxidation of Al_2O_3 can provide additional protection [46], [47], [50]. However, if the core temperatures continue to rise as might happen in a beyond design basis accident (BDBA) scenario, this protective Al_2O_3 shell eventually fails and a sudden rapid increase in oxidation occurs

as the underlying FeCrAl begins to react. This 'breakaway oxidation' has been observed experimentally to occur very close to the melting point of FeCrAl at around 1500°C (1773 K), although this depends on which FeCrAl alloy is under consideration [44], [51], [52], [53] as discussed further in Section 3. This complex oxidation behavior enables the benefits of FeCrAl as an ATF material, and yet also makes accurate modelling a challenge in BDBA or severe accident simulations. An appreciable drawback of FeCrAl is the neutronic penalty associated with its use, which increases the required fuel enrichment, although this can be substantially mitigated by reducing the clad thickness and hence increasing the fuel loading through making the pellet slightly bigger [54].

2 MELCOR PWR Model

2.1 Description of MELCOR Model

A MELCOR model of the Zion reactor developed for MELCOR 1.8.5 was provided by the NRC. This model has been used in previous work to simulate an LBLOCA and station blackout accident scenario [55], [56]. The legacy model was used as a template for a new MELCOR model of the Zion reactor using the more recent MELCOR 2.2, which has some important differences in the input file format compared with MELCOR 1.8.5 [40]. The geometry in the new MELCOR 2.2 Zion model was also changed from 15 × 15 fuel pin lattice to a 17 × 17 layout to reflect a typical 4 loop PWR.

The MELCOR radial and axial nodalization schemes are shown in Figure 1. The fuel pin surface areas, UO_2 fuel and clad masses, and inter-pin flow areas were recalculated using the new 17 × 17 clad outer radius as shown in Table 2. It should be noted that, for the original 15 × 15 model, the fuel-clad gap was smeared into the clad material and not modelled as a separate region.

Table 2: Fuel geometric parameter comparison between 15 × 15 and 17 × 17 assemblies.

Parameter	Units	15 × 15	17 × 17
Fuel pin radius	mm	4.647	4.095
Fuel-clad gap thickness	mm	0.000	0.085
Clad inner radius	mm	4.646	4.180
Clad outer radius	mm	5.359	4.750

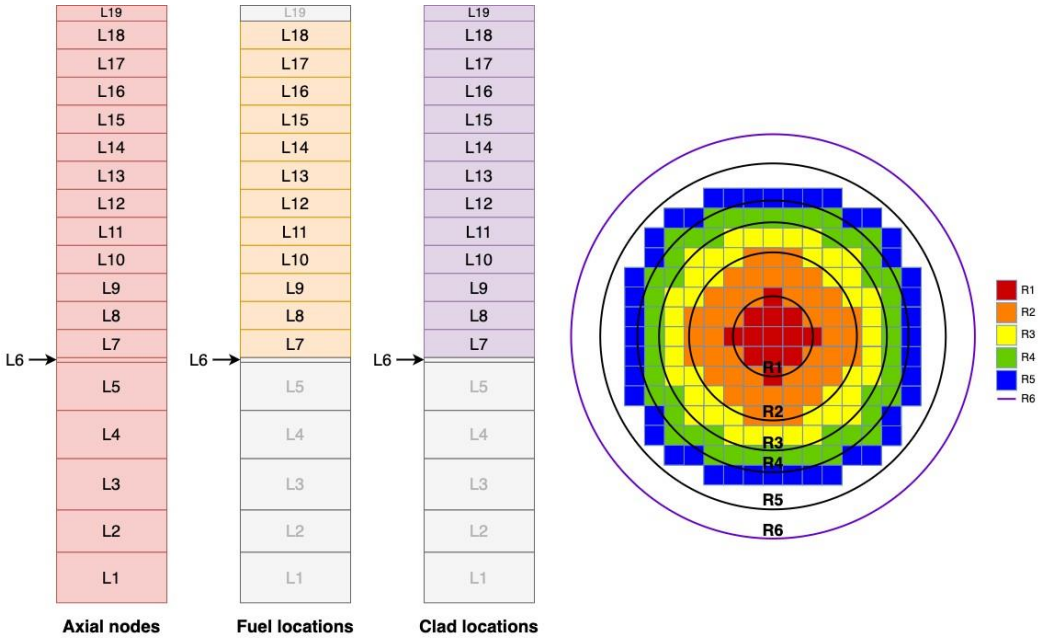

Figure 1: Axial and radial nodalization scheme used in MELCOR.

The systems model of the reactor is shown in Figure 2. MELCOR constructs a list of control volumes containing important systems, defines flow paths between these volumes, and specifies materials and interactions occurring in the plant.

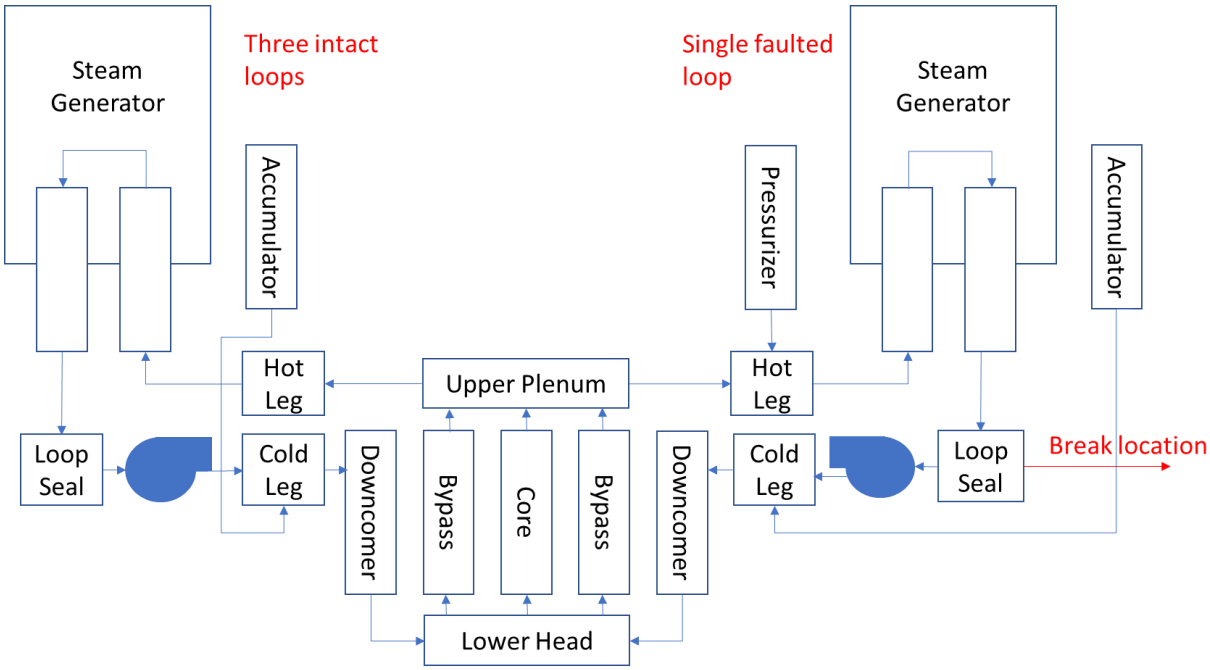

Figure 2: MELCOR ZION model control volumes [55], [56]

The predefined LBLOCA scenario in the ZION model consists of a double-ended guillotine rupture of the pressurizer loop at the inlet to the reactor coolant pump, causing the reactor to scram. The Emergency Core Cooling System (ECCS) Low Pressure Safety Injection (LPSI) is prevented from activating at the beginning of the accident, leaving the core vulnerable to uncovering and damage as the coolant escapes. However, as this model was originally developed to support the calculation of the source term specifically for *recovered* LOCAs, the LPSI system is assumed to be recovered (i.e., by manual startup) by operators 27 minutes after reactor scram. The model was originally developed by Brookhaven National Laboratory [57] and subsequently modified by Sandia National Laboratories as part of an assessment of the application of NUREG-1465 [58] on population dose for recovered LOCAs, and this recovery time was hence specified a priori [55]. This case is of particular interest with FeCrAl clad, as this has the potential to delay (although not ultimately prevent) the onset of core melt, hence reducing the fission product release; therefore, reducing the source terms in recovered LOCAs. An illustration of the LBLOCA scenario timeline is shown in Figure 3.

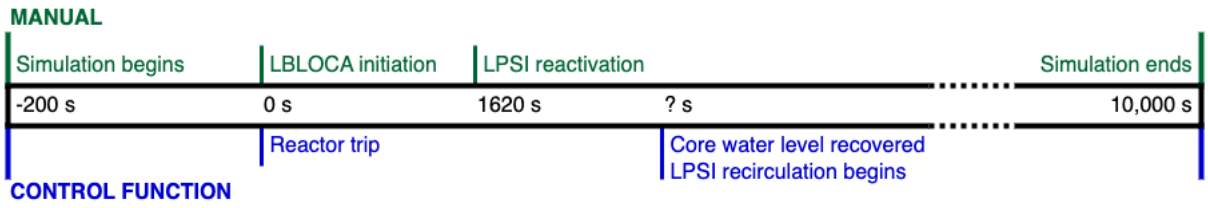

Figure 3: MELCOR LBLOCA accident sequence

The manually defined events occurring at specific times in the scenario are shown in green along the top of the timeline, while the MELCOR 'control functions' which are triggered when set conditions are met are labelled along the bottom in blue. The simulation begins 200 seconds before the initiation of the accident, providing a period of normal operational data before the LBLOCA. The rupture of the pressurizer loop is instigated at 0 seconds, which triggers a reactor trip and shutdown. However, the lack of immediate LPSI injection activation results in a lack of proper core cooling after shutdown. In the NRC scenario provided and used in previous work, the LPSI successfully re-activates after 1620 seconds (27 minutes). Once the core water level has risen to cover the core once again the LPSI control function switches from recovery injection to recirculation mode. The simulation continues until 10,000 seconds to capture the aftermath of the accident and final state of the reactor.

The results from the updated 17 × 17 model run in MELCOR 2.0 were compared with the results from the original 15 × 15 model using MELCOR 1.8.5 for the standard Zr clad. This comparison is presented in the following subsection. An additional model was then created using FeCrAl ATF instead of Zr for the clad material, which is presented in Section 3.

2.2 Model Verification

The MELCOR 2.2 with Zr-clad fuel model results are compared with the SNL/NRC results for MELCOR 1.8.5 and 2.0 [55], [56], with selected results for MELCOR 2.2 in Figure 4 – Figure 6. The unaltered MELCOR input (with 15 × 15 fuel) was first run to quantify differences between MELCOR versions. Some differences are to be anticipated due to the continued evolution of the code and the sensitivity of outcomes in beyond-design basis accidents to relatively small variations in conditions and assumptions. The updated model with 17 × 17 Zr-clad fuel is then run, and the results compared to the original 15 × 15 model. Only the results from MELCOR 2.2 (generated in this paper) are shown. The reader is referred to Ref. [55], [56] for graphical results with the previous versions of MELCOR, and a summary of the comparison is given below. In this analysis, the MELCOR default fission product inventory with the ANS standard decay heat curve [59] is used, with a 3250 MWth core power, for consistency with the original analysis.

The core water level of all models dropped below the top of the active fuel, with the 2.2 results showing a drop of around 3 m in a behavior that is more similar to the drop and recovery of the 1.8.5 water level results than the 2.0. The water level in the 2.2 results notably does not recover fully to stay above the level of the active fuel. The containment pressure for the 2.2 model matches well with the 2.0 results, including the rise when the containment sprays switch from injection mode to recirculation mode.

The fuel temperature shows different behavior in the 2.2 results, with fuel melting not penetrating as far down as seen for the 2.0 model. In the 2.0 results, fuel melting reaches axial levels L8 and L9, whereas the 2.2 results do not observe fuel melting until L11 for the 15 × 15 model and L12 for the 17 × 17 model. It is unknown from the previous results which axial level the 1.8.5 model fuel melt reaches. Higher fuel melt is seen for 17 × 17 fuel than for the 15 × 15 fuel, but it is noted that the clad temperatures are very similar, indicating sensitivity to small changes in initial conditions. This is known to be a feature of severe accident analysis and hence the increased fuel melt could perhaps be due to thinner clad.

The hydrogen production results for 2.2 match well with the previous MELCOR results, which observed a range of around 240 – 275 kg between 1.8.5 and 2.0. Less hydrogen is produced for the 15 × 15 model than for the 17 × 17 model, which could be due to the larger pin surface area or the longer time the fuel in the 17 × 17 model is uncovered. The total radioactive mass released from the core in the 2.2 model is consistent with previous results.

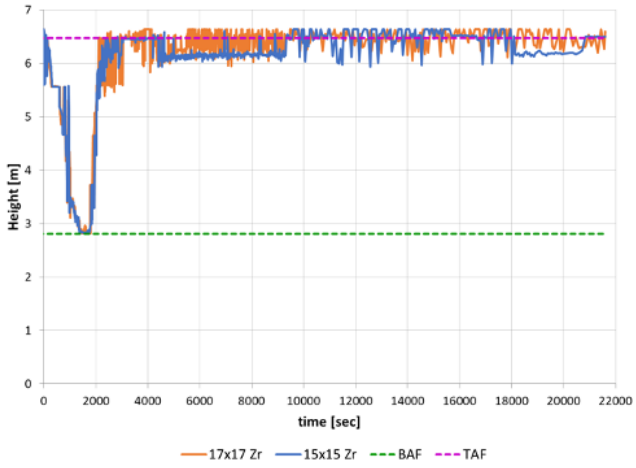

Figure 4: Core water level in MELCOR 2.2 (dotted lines indicate top and bottom of active fuel)

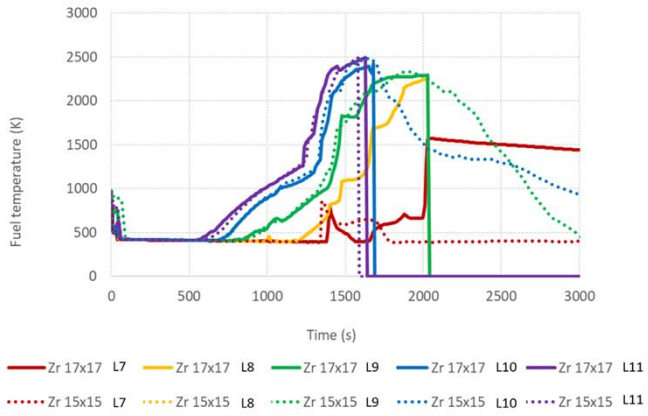

Figure 5: Fuel temperature in MELCOR 2.2

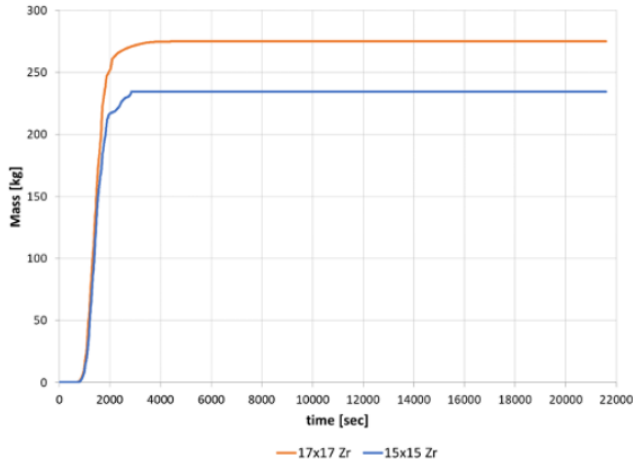

Figure 6: Hydrogen production in MELCOR 2.2

3 MELCOR FeCrAl modeling

3.1 FeCrAl UDM definition

While previous work investigating FeCrAl using MELCOR has needed to redefine the default Zry clad material to use FeCrAl properties, this work used the new UDM capability to explicitly define the FeCrAl metal clad and the oxide produced when this clad undergoes oxidation during the LBLOCA [25], [26].

The UDM method defines a new material within the MELCOR Material Properties (MP) package. Four new materials may be created: two generic materials, one metal, and one oxide of that metal. Each is initialized using a default material as a base, with a set of default molten material properties taken as specified in Table 3 below. These include the coefficient of thermal expansion β, molar specific volume v_{mol}, and the coefficients *ALPHI* and *OXMUI* which are used to calculate the viscosity of the molten material.

Table 3: MELCOR UDM default materials and default molten material properties

UDM	Default material	β $(1/\mathrm{cm}^3)$	v_{mol} $(\mathrm{cm}^3/\mathrm{mol})$	*ALPHI* (K)	OXMUI $(\mathrm{Pa}\cdot\mathrm{s})$
COR-USER1	Stainless steel	3.10×10^{-5}	7.7	3313	1.08×10^{-3}
COR-USER2	Stainless steel	3.10×10^{-5}	7.7	3313	1.08×10^{-3}
COR-USER-METAL	Zircaloy	1.65×10^{-5}	15.7	3313	1.08×10^{-3}
COR-USER-OXIDE	Zirconium oxide	5.88×10^{-5}	23.48	4620	9.80×10^{-3}

The UDM is initialized using these parameters but the user may edit and redefine every property to more accurately model the desired material. In this work the final two UDMs were added and redefined to replicate

FeCrAl and FeCrAl Oxide. Where no reliable source is found for C26M, generic FeCrAl properties have been used; where no reliable FeCrAl source is found, the UDM reverts to the stainless steel defaults.

As FeCrAl properties are less well-known than Zircaloy behaviors, there is some uncertainty in the experimental data and some institutions report slightly different results to others. Uncertainty and sensitivity analysis is planned for future work, although comparison between C26M and another FeCrAl alloy, Kanthal APMT [60], is made in this paper.

3.1.1 Dynamic viscosity

Dynamic viscosity information is required in MELCOR when a material becomes molten. MELCOR requires the dynamic viscosity and thermal expansivity for a metal to be input directly. The dynamic viscosity μ_i of an oxide material i is calculated using the empirical coefficients $ALPHI$ and $OXMUI$ in an Arrhenius form:

$$\mu_i = OXMUI \cdot exp\left(\frac{ALPHI}{T}\right) \tag{1}$$

Due to the lack of available data for these parameters for FeCrAl and FeCrAl oxide, the default MELCOR values for stainless steel have been used. The dynamic viscosity required for FeCrAl was calculated using the FeCrAl melting temperature of 1773 K and the stainless steel defaults given in the MELCOR User Guide to solve Equation 1.

3.1.2 Emissivity

For a linear relation the emissivity, ϵ is calculated in MELCOR using the zero-temperature emissivity, A, and the emissivity gradient, B:

$$\epsilon = A + BT \tag{2}$$

There is a lack of exact data for C26M FeCrAl and FeCrAl oxide emissivity, but the Kanthal APMT datasheet gives the maximum bound as 0.7 [47]. This is taken as the upper bound of the FeCrAl emissivity, with the rest of the data taken from the MELCOR User Guide FeCrAl/FeCrAl oxide example [25], [26]. This is deemed acceptable given that previous work has used the same emissivity relation for FeCrAl/FeCrAl oxide as Zr/ZrO, changing only the maximum emissivity bound from 1.0 to 0.7 [28], and as varying emissivity parameters is expected to have a small effect on heat transfer.

3.1.3 Summary

The material properties used are detailed in Table 4, along with references for each parameter.

Table 4: Material properties used in MELCOR model.

Parameter	Units	FeCrAl	FeCrAl Oxide	Reference and Notes
Density	kg/m^3	7100	5180	[61], [62], [63]
Melting point	K	1773	1901	[61], [62], [63]
Latent heat of fusion	J/kg	270,000	687,463	[25], [26]
Dynamic viscosity	Pa·s	6.972×10^{-3}	-	Default for steel [25], [26]
Thermal expansivity per mol. vol.	$K^{-1}\cdot cm^{-3}$	-	2.387×10^{-4}	Default for steel [25], [26]
$ALPHI$ (Eq. 1)	K^{-1}	-	3313	Default for steel [25], [26]
$OXMUI$ (Eq. 1)	Pa·s	-	1.076×10^{-3}	Default for steel [25], [26]
Emissivity bounds	-	0.0~0.7	0.0~0.7	Kanthal APMT maximum [47]
A (Eq. 2)	-	4.200×10^{-2}	0.7	FeCrAl/FeCrAl oxide example [25], [26]
B (Eq. 2)	-	3.474×10^{-4}	0.0	FeCrAl/FeCrAl oxide example [25], [26]

3.2 Temperature-dependent properties

The FeCrAl UDM specific heat, thermal conductivity, enthalpy, and density parameters are defined in MELCOR tabular functions with respect to increasing temperature. This allows the UDM to more accurately capture the behavior of FeCrAl and FeCrAl Oxide over the range of temperatures seen throughout the accident scenario. The data is taken from a combination of the ORNL handbooks on FeCrAl and various reports [28], [45], [61], [64]. While detailed data specific to C26M is limited, results from other low-Cr FeCrAl alloys and APMT where necessary have been used to fill in the gaps in the same manner as previous work [18]. The properties are shown in Figure 7 below, with references and discussion following.

Figure 7: Thermal properties of FeCrAl used to approximate C26M in this work.

3.2.1 Specific heat

The specific heat of C26M has been investigated by ORNL in a series of experiments using the C26M2 alloy [45]. The results are shown in Figure 8. One interesting behavior of C26M observed by ORNL is the difference between the results when heating and cooling the specimens. The cause of this discrepancy, which becomes larger at higher temperatures, has been hypothesized to be microstructural changes which occur during exposure and could affect the coefficient of thermal expansion thereafter. This may be something to include in future analysis as ORNL identified the effect in three different test samples, suggesting that it is an accurate representation of the behavior of C26M thermal properties.

The C26M2 results [45] were found to follow the same correlations used for the specific heat of other FeCrAl alloys in MELCOR. These are shown below, where T_c is the Curie temperature (reported as ~853 K) and T_m the melting temperature:

$$c_p = aT + bT^2 + cT^3\,, \quad T \le T_c \tag{3}$$

$$c_p = aT + bT^2 + cT^3 + \frac{D}{T} + E\ln\left(\frac{abs\,(T - T_c)}{T_c}\right), \quad T_c < T < T_m \tag{4}$$

Figure 8 shows the polynomials fit using the reported coefficients for C35M [61]and C36M (dashed lines) compared with the experimental results from C26M2 (solid lines). It may be seen that the C35M fit better matches the C26M2 results. These C35M coefficients were therefore used in this work to approximate the C26M specific heat variation with temperature.

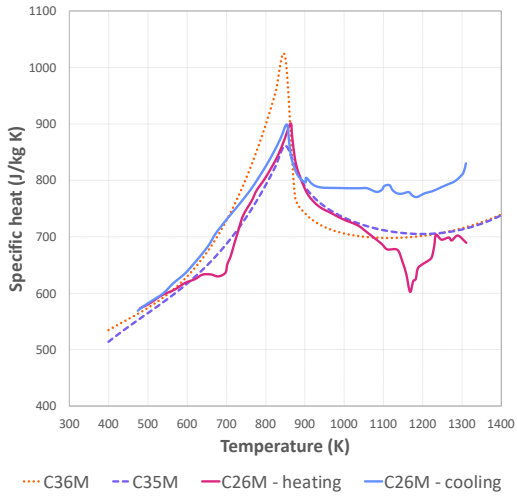

Figure 8: Specific heat capacity of C26M2 as a function of temperature, as reported in [45], compared with polynomial fits derived for C35M and C36M reported in [61]

3.2.2 Thermal conductivity

As data for the thermal conductivity of C26M was not available, the closest match reported in the ORNL 2018 Handbook on the Material Properties of FeCrAl was used [61]. The thermal conductivity κ for is calculated using the following relation:

$$\kappa = A_1 T^2 + A_2 T + A_3$$

where $A_1 - A_3$ are the reported fitting constants for C35M, in order to maintain consistency with the specific heat capacity results. Note that no range of validity is provided for the thermal conductivity and there is some extrapolation here above the experimental data (300-1400K) up to the melting point (1773K). As no limit to the range of validity is given in the ORNL Handbook, the goal of this calculation is best estimate, and the trend is linear, it was considered reasonable to extrapolate rather than apply a cutoff value at 1400K.

3.2.3 Enthalpy & density

No data on the temperature dependence of the specific enthalpy or density for FeCrAl was found for C26M in either the surveyed literature or the ORNL 2018 Handbook. Data from an older ORNL report using Kanthal APMT properties was used [28].

3.3 Oxidation behaviors

One of the key effects to capture when considering FeCrAl clad is the oxidation behavior during an accident. As discussed previously, the preferential oxidation of aluminum at temperatures above operational but below about 1350°C leads to the formation of a protective Al_2O_3 scale on the outer surface of the clad. The slow oxidation at the beginning of the accident due to this effect, as well as the rapid increase in oxidation after the failure of this scale, are crucial to understanding the behavior of FeCrAl ATF in an accident scenario.

The MELCOR UDM capability allows the explicit definition of oxidation reactions for each element in an alloy, enabling a level of precision oxidation modeling which has not previously been possible in FeCrAl simulations. Previous work without the UDM capability has been required to simplify oxidation effects by considering the oxidation rate of the clad as a whole rather than on an elemental basis [61], [65]. The UDM model enables the oxidation reactions to be considered separately and with individually specified parabolic rate equation constants, coefficients, and temperature ranges.

The oxidation reactions for each element in FeCrAl clad are defined in Equations 5 – 7, each with an associated heat of reaction, Q_{ox}.

$$\mathrm{Fe + H_2O \rightarrow FeO + H_2} + Q_{ox} \quad (5)$$

$$\mathrm{Cr + 1.5\ H_2O \rightarrow 0.5\ Cr_2O_3 + 1.5\ H_2} + Q_{ox} \quad (6)$$

$$\mathrm{Al + 1.5\ H_2O \rightarrow 0.5\ Al_2O_3 + 1.5\ H_2} + Q_{ox} \quad (7)$$

These molar equations are defined in the MELCOR COR package, along with the value of Q_{ox} for each case as reported in the National Institute for Standards and Technology thermochemical database [66]. The oxidation rate coefficients for each element are then specified, following the parabolic rate equation described in Equation 8.

$$k_P = k_0 \exp\left(-\frac{E_a}{RT}\right), \qquad T_{min} \leq T \leq T_{max} \tag{8}$$

where k_P is the reaction rate constant with respect to the metal reacted, k_0 is the mass gain rate constant, E_a is the activation energy, and R is the gas constant, and T is the temperature within the range of validity T_{min} to T_{max}. The mass gain rate constant k_0 for FeCrAl is taken as 784.0 kg^2/m^4s from Pint [50], [53]. However, this value is for the mass of oxide produced rather than the mass of each individual metal reacted. The latter are the parameters required by MELCOR. Care must be taken to convert the literature data into the correct format, as has been observed by others using MELCOR [67]. Each individual elemental contribution may be found by taking the ratio of each metal present in FeCrAl (as described in Table 1).

A mole-weighted approach for the heat of reaction for the oxidation of FeCrAl was taken rather than the FeCrAl heat of reaction (e.g. as in Ref. [68]), where the heat of reaction for each constituent element is weighted according to the molar composition of the alloy. This allowed the oxidation reaction of each of the constituents to be handled separately in calculating the hydrogen generated.

The Al_2O_3 layer formation and the subsequent 'breakaway oxidation' occurring when this protective scale fails are modeled using Equation 8 with two different temperature ranges above and below the designated breakaway oxidation temperature. In the lower temperature range oxidation is dominated by Equation 7 as the Al_2O_3 shell forms. In the higher temperature range the default oxidation data for stainless steel is used as once the Al_2O_3 shell fails, FeCrAl oxidation is dominated by Fe in the same manner as stainless steel. This approach has been widely used in past analysis with good results [28], [65], [69].

The main difference between the two FeCrAl alloys considered in this work, C26M and APMT, appears to be the temperature at which breakaway oxidation occurs. Initial experiments show a range of breakaway oxidation temperatures and there is significant uncertainty in the exact temperature for each alloy. At lower temperatures between 800°C and 1300°C, C26M and APMT have been shown to exhibit almost identical oxidation behaviors [44], [70]. However, at higher temperatures the oxidation behavior of the two alloys seems to diverge. Experiments seem to show a higher breakaway oxidation temperature for high-Cr APMT and a lower breakaway oxidation temperature for lower-Cr alloys such as C26M.

Pint et al. performed experiments to investigate the high-temperature behavior of FeCrAl alloys in both air and steam conditions [51]. The Al_2O_3 shell formed by the high-Cr APMT was observed to fail at temperatures exceeding 1500°C, while the low-Cr alloys considered (B136Y and C135M) saw shell failure and the onset of breakaway oxidation from 1400°C onwards. ORNL experiments using B136Y observed swift Al_2O_3 shell failure and breakaway oxidation at 1475°C [65], while Dryepondt et al. observed high specimen mass changes indicating breakaway oxidation at 1450°C for a variety of low-Cr alloys [71]. In their review of available literature and experimental data for ATF concepts, PNNL note the apparent effect of material composition on the high-temperature steam oxidation resistance for FeCrAl [72]. Breakaway oxidation was observed at temperatures above 1400°C in Ref. [73].

This difference in oxidation behavior is captured in the MELCOR model by using two different breakaway oxidation temperatures in the high-temperature regime prescribed for the UDM FeCrAl oxidation model. These are shown in Table 5 below.

Table 5: MELCOR material oxidation behaviors.

Material	Temperature range (K)	Behavior
Zry	1100 – 9900	MELCOR default Zry oxidation behavior.
FeCrAl APMT	1100 – 1773	Oxidation dominated by Al_2O_3 reaction.
	1773 – 9900	Breakaway oxidation occurs at 1773 K, stainless steel default used to show switch to FeO-dominated regime.
FeCrAl C26M	1100 – 1748	Oxidation dominated by Al_2O_3 reaction.
	1748 – 9900	Breakaway oxidation occurs at 1748 K, stainless steel default used to show switch to FeO-dominated regime.

3.4 Eutectic interactions

MELCOR models molten material as a conglomerate debris mixture of material from different core components. Material can enter the conglomerate debris as a liquid produced from a material reaching its associated melting temperature, as when C26M FeCrAl clad reaches 1773 K; as a product of a eutectic interaction between two materials reaching their defined eutectic temperature, as when ZrO_2 and UO_2 are in contact and reach 2800 K; or as a solute in a known liquid solvent, as when molten Zry clad material dissolves UO_2 fuel. MELCOR contains a dedicated model to capture eutectic interactions between ZrO_2 and UO_2 but there are no current capabilities to model any eutectics occurring with FeCrAl clad as a UDM. Due to this constraint, the eutectic model has not been used for this work and the default melting behavior is observed for both FeCrAl and UO_2 clad.

3.5 Clad burst

MELCOR includes a detailed modeling of Zry-clad failure mechanisms. The most relevant in this work are the rod burst, hold-up by oxide shell, and eutectic reactions.

The rod burst and radionuclide release to the gap is assumed to occur at 900°C (1173K), which is consistent with previous work [65], [74]. It is noted that recent experiments have shown that C26M bursts at temperatures ~150-250°C higher than Zry due to its superior mechanical strength [75]. This could be considered in future studies. For the transient considered here, the impact of rod burst temperature on fission product release is small, as the transient is sufficiently severe that most of the core will experience gap release in any case and a substantial fraction of the core melts.

The hold-up by oxide shell model aims to capture the mechanical effect of the outer shell formed around the Zry clad when oxidation occurs with steam. This oxide shell has a higher melting temperature than the underlying clad and has been observed to maintain structural integrity even as the unoxidized clad material inside the shell melts away [76]. MELCOR allows a ZrO_2 shell to remain intact and able to support a melt up to 2400 K, after which a time-at-temperature failure mode was activated, and the clad begins to fail. If the temperature reaches 2800 K, instant failure and collapse of the oxide shell is assumed. However, as this effect is not expected to be observed in FeCrAl clad [51], [65], the failure temperature for both shell hold-up and collapse is modeled as the oxide melting temperature for FeCrAl. This data is displayed in Table 6.

Molten Zry clad also reacts strongly with the oxide shell and the UO_2 fuel pellet itself in a eutectic reaction [77]. The eutectic material formed has an effective liquification temperature that is lower than the melting temperature for either material individually. The eutectic formation temperature for ZrO_2 with UO_2 is 2450 K rather than the measured melting points of 2990 K and 2800 K, respectively [25], [26]. This informs the shell melt hold-up temperature given in Table 6 and may be included in MELCOR via the activation of a specific eutectics model of material interactions.

Table 6: MELCOR material failure temperatures

Material	Rod Burst Onset (K)	Melting		Oxide Forced Failure	
		Metal (K)	Oxide (K)	Shell Melt Hold-up (K)	Collapse (K)

Zry	1173	2098	2990	2400	2800
FeCrAl	1173	1773	1901*	1901	1901

*Note that Ref. [78] also considered a range from 1870-1973K

4 Modelling of HBU Fuel

4.1 Depletion Calculations of Equilibrium Cycle

To prepare the accurate EOEC fission product inventories and decay heat profiles for the FeCrAl and Zry MELCOR models, detailed equilibrium cycle depletion calculations are required. In this work, a previously developed and verified whole-core PWR model [79] was leveraged to generate required quantities of interest using VERA [80]. This four-loop model, which uses Zircaloy as the clad materials and features an 18-month cycle length, is based on the Watts Bar Nuclear Unit 1 reactor, comprised of 193 fuel assemblies with a core power of 3411 MWth. The assembly design follows a 17×17 lattice, which is consistent with the modified MELCOR model (see above), and small deviation in the thermal output is considered acceptable in this scoping study. Two equilibrium cycle core designs were determined for the FeCrAl cladded fuel using VERA with the cycle length of 18 and 24 months, respectively.

Here the fuel geometry was assumed identical in both cases, including the clad thickness. It is noted that the reactivity penalty from FeCrAl can be reduced by making the clad thinner, made possible by its higher mechanical strength. This slightly decreases the reactivity penalty but allows the fuel pin diameter and therefore mass to be slightly increased thus allowing the enrichment penalty to be significantly reduced. This was not considered here. Changing the clad thickness is not anticipated to significantly affect results as the fission product inventory, decay heat and fuel pin surface area would not be affected [54].

To mitigate the computational burden associated with the high-order transport method used for solving the 3-D reactor core problem, the so-called “jump-in” technique was leveraged in VERA cycle depletion calculations to determine the equilibrium core design as quickly as possible. This technique uses the irradiation history of each fuel assembly type calculated individually to approximate the outcome of the previous cycle’s full-core simulation results. The process involves three fundamental steps. First, depletion calculations are performed for each fuel assembly type for all previous cycles. Second, a full-core fuel shuffling calculation is performed using the results obtained from the individual fuel assembly depletion calculations. Finally, full-core depletion calculations are executed to determine and establish the equilibrium cycle. This technique allows an accurate irradiation history for the full-core equilibrium cycle to be computed and the semi-optimal core design to be determined at a reduced computational cost.

The resulting core loading patterns for the 18-month and 24-month using FeCrAl clad are illustrated in Figure 9. Both of them are 2-batch cores following the low leakage loading pattern with the burned assemblies at the periphery of the core. The specifications of the number, type, and enrichment of the fuel rods used in each design are detailed in Table 7. There is an increase in the burnable poison loading for this design as this is needed to combat the increased boron concentration, which in turn is brought about by the increased fuel enrichment and initial reactivity values with a selection of assembly design options to improve the equilibrium cycle length. The core average EOEC burnup was found to be 33.2 GWd/t and 45.1 GWd/t for the 18-month and 24-month cycle, respectively, with FeCrAl cladded fuel.

Figure 9. Core loading pattern for 18-months (right) and 24-months (left) designs.

Table 7 Assembly design options for the 18-month and 24-month core design

Loading Batch	18-month Core Design			24-month Core Design		
	Enrichment (wt.%)	No. IFBA*	No. WABA**	Enrichment (wt.%)	No. IFBA	No. WABA
a	5.2	104	0	7.05	200	0
a	5.2	200	0	7.05	200	24
b	5.7	200	0	7.55	200	0
b	5.7	128	0	7.55	200	24
b	5.7	128	24			

*IFBA: Integral Fuel Burnable Absorber
**WABA: Wet Annular Burnable Absorber

Table 8 compares the equilibrium cycle performance of the two core designs. The pinwise 3-D core power distribution was converted into an RZ nodalization for use in MELCOR.

Table 8: Equilibrium cycle performance of 18-month and 24-month with FeCrAl Clad

Core Parameters	**18-month FeCrAl**	**24-month FeCrAl**
Cycle burnup (GWD/MTU)	19.596	26.840
Cycle length (EFPD)	510.2	697.4
Peak pin burnup (GWD/MTU)	58.56	81.87
Peak assembly burnup (GWD/MTU)	55.31	77.85
Peak boron concentration (ppm)	1298	1281
Enthalpy rise hot channel factor ($F_{\Delta H}$)	1.621	1.614
Heat flux hot channel factor (F_Q)	1.92	2.05

4.2 Derivation of MELCOR Fission Product Inventories

SCALE [81], [82] was used to provide accurate EOEC fission product inventories and decay heat profiles for the FeCrAl and Zry MELCOR models. A single-assembly SCALE calculation at the core average enrichment was then performed to burn the fuel to the EOEC core average burnup. This introduces an approximation as the

most accurate method would be to produce SCALE models for every burnup zone in the core. However, the great complexity added by this method produces only a small effect on the results and therefore the core average burnup approximation was implemented. The SCALE POLARIS method of characteristics solver was used with the embedded self-shielding method to allow rapid, robust specification of the assembly and the use of appropriate default solver options. The calculation was performed with 56 energy groups as this provided suitable accuracy while reducing runtime. The assembly geometry in quarter-symmetry is shown in Figure 10.

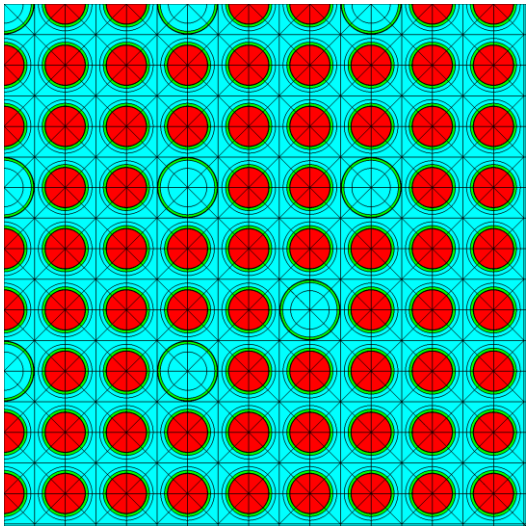

Figure 10: Assembly geometry used in SCALE calculation, with quarter symmetry.

MELCOR defines 17 DCH/RN ‘classes’, each containing a set of elements with similar behavior to a specific ‘header element’. These classes are shown in Table 9.

Table 9: MELCOR decay heat and radionuclide classes

Number	Chemical Group	Header Element	Elements
1	Noble gases	XE	Xe, Kr, Rn, He, Ne, Ar, H, N
2	Alkali metals	CS	Cs, Rb, Li, Na, K, Fr, Cu
3	Alkaline earths	BA	Ba, Sr, Be, Mg, Ca, Ra, Es, Fm
4	Halogens	I2	I, Br, F, Cl, At
5	Chalcogens	TE	Te, Se, S, O, Po
6	Platinoids	RU	Ru, Pd, Rh, Ni, Re, Os, Ir, Pt, Au
7	Transition metals	MO	Mo, Tc, Nb, Fe, Cr, Mn, V, Co, Ta, W
8	Tetravalents	CE	Ce, Zr, Th, Np, Ti, Hf, Pa, Pu, C
9	Trivalents	LA	La, Pm, Sm, Y, Pr, Nd, Al, Sc, Ac, Eu, Gd, Tb, Dy, Ho, Er, Tm, Yb, Lu, Am, Cm, Bk, Cf
10	Uranium	UO2	U
11	More volatile main group metals	CD	Cd, Hg, Pb, Zn, As, Sb, Tl, Bi
12	Less volatile main group metals	AG	Sn, Ag, In, Ga, Ge
13	Boron	BO2	B, Si, P
14	Water	H_2O	'WT'
15	Concrete	CON	'CC'
16	Cesium iodide	CSI	-
17	Cesium molybdate	CSM	-

The initial mass and specific decay heat for each element are defined individually in the DCH package, using the data provided by SCALE. The classes are then defined by their respective constituent elements and weighted by their initial mass at the time of shutdown. The whole-core decay power was calculated by SCALE and defined explicitly as an input tabular function in MELCOR.

Classes 16 and 17 are added to account for the cesium iodide and cesium molybdate compounds, which must be modelled individually to accurately capture the more volatile behavior they exhibit. The distribution of iodine, cesium, and molybdenum across the CS, I2, MO, CSI, and CSM classes is calculated using information from Sandia National Laboratory reports on decay heat and radionuclide inventory definitions for severe accident simulations [83], [84], [85], as described below and illustrated in Figure 11 – Figure 14.

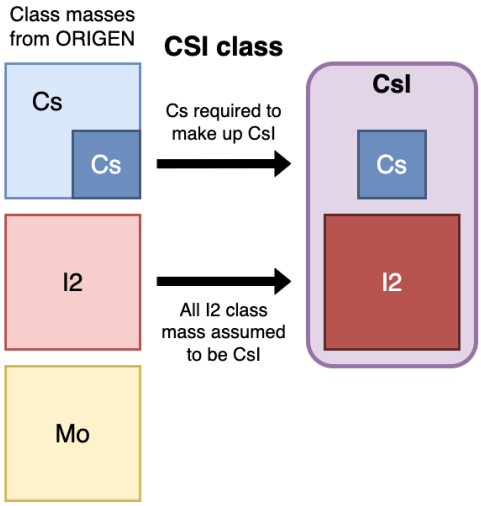

Figure 11: CSI class definition

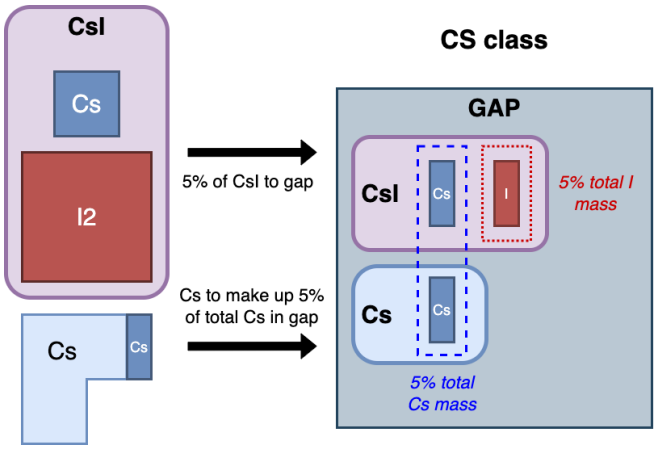

Figure 12: CS class definition

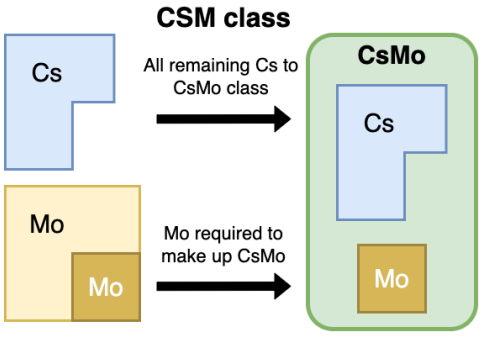

Figure 13: CSM class definition

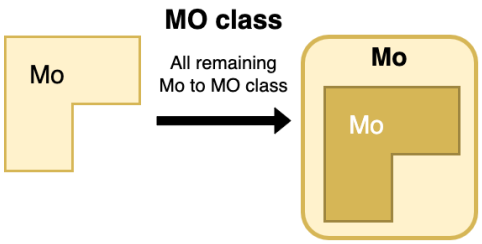

Figure 14: MO class definition

For the CSI class, the total mass of iodine in the core is assumed to be present as cesium iodide. The corresponding mass of cesium required to make up the compound is calculated using the ratio of 0.51155:0.48845 Cs:I defined in the SOARCA work as the MELCOR best practice [76]. This cesium mass is subtracted from the total element mass and added to the cesium iodide class.

The CS class is used purely for the cesium present in the fuel-clad gap. The gap fractions of cesium and iodine are defined by the SOARCA best practice as 5% of their total mass, which means we must calculate the contributions from both cesium iodide and pure cesium. The mass of iodine in the gap may be easily calculated by taking 5% of the iodine in the cesium iodide class, as this now contains all the iodine present in the reactor. This is added to the gap in the RN package. The amount of cesium included in the CSI class gap contribution is then calculated by the script, and the additional cesium mass required to make this up to 5% of the total cesium mass is found. This cesium mass is added to the CS class, all of which is added to the gap in the RN package.

The remaining cesium mass left after the CSI and CS class contributions have been subtracted is all assumed to be present as cesium molybdate. The corresponding mass of molybdenum required to make up the compound is calculated using the ratio of 0.734789:0.265211 Cs:Mo defined in the SOARCA best practice. This molybdenum mass is subtracted from the total element mass and added to the cesium molybdate class. The remaining molybdenum mass is then allocated to the molybdenum class, MO.

The distribution of the fission product inventory across the core is defined in the RN package using the axial and radial power distributions from VERA, as discussed in Section 1.3. The MELCOR calculation results for these 17 DCH/RN classes are sent to MACCS for use in source term calculations.

5 MELCOR Results & Discussion

5.1 Clad temperature and core damage

The clad temperature and extent of core melt are first investigated. These are not the primary simulation output but are useful in understanding the transient. All regions of the core experience an increase in clad temperature prior to the LPSI being restarted. This rise is quicker for the Zry case due to the oxidation reaction, although this is somewhat mitigated by the higher melting temperature of zircaloy compared to FeCrAl. In all cases, the central radial node of the core experiences complete failure, with the clad melting throughout this region. In other rings, the upper part of the core melts while the lower part generally survives. Note that in the following figures, the axial layers are numbered as shown in the diagram in Figure 1, with L7 the bottom and L18 the top of the fuel regions. A sharp drop in clad temperature to zero indicates that the clad in the specified node has collapsed. There are ‘cliff edge’ effects that contribute to the degree of core melt, discussed further below.

The APMT case exhibits appreciably lower core melt than the Zry and C26M cases, which are similar. This is illustrated for the third ring of the core (R3 in Figure 1) partially melts for the 18 month (18m) Zry case (Figure 15) but survives for the APMT cases (Figure 16 and Figure 17).

The fourth ring (R4 from Figure 1) of the Zry core narrowly avoids melting (Figure 18**Error! Reference source not found.**). However, for the C26M cores this ring partially melts around the same time the LPSI reactivates (Figure 19 and Figure 20), likely driven by breakaway oxidation immediately prior to quenching. This suggests sensitivity both to the C26M material parameters and LPSI reactivation time. Additionally, very small changes to the simulation parameters (e.g., a change of order ~0.01%) can cause significant changes in the melt behavior – for example they can cause the entire second ring of the Zry core can melt after the LPSI reactivates.

The sensitivity of the core melt to exact simulation parameters is a known feature of severe accident simulations, which exhibit strong nonlinear behavior. The sensitivity of the fission product release and hydrogen production (the key output variables) to the exact simulation inputs is much lower than for the core melt. However, this behavior does nonetheless motivate sensitivity and uncertainty analysis, which will be performed in future work.

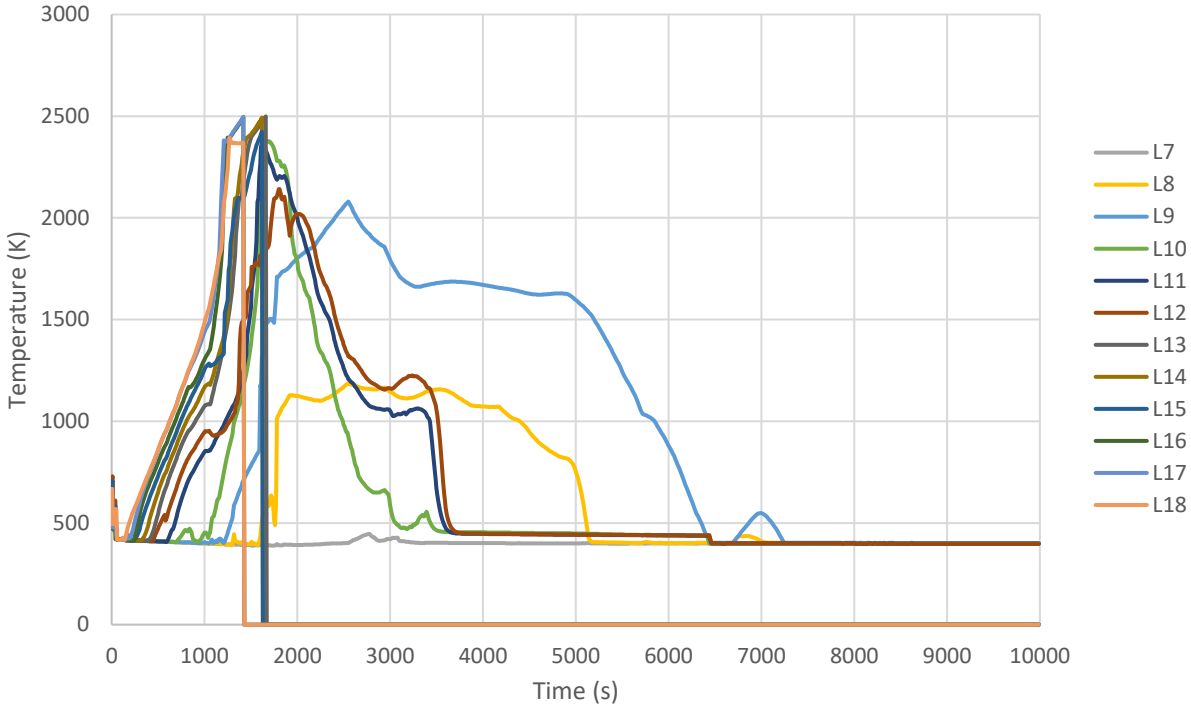

Figure 15: Zry 18m clad temperature in third radial zone

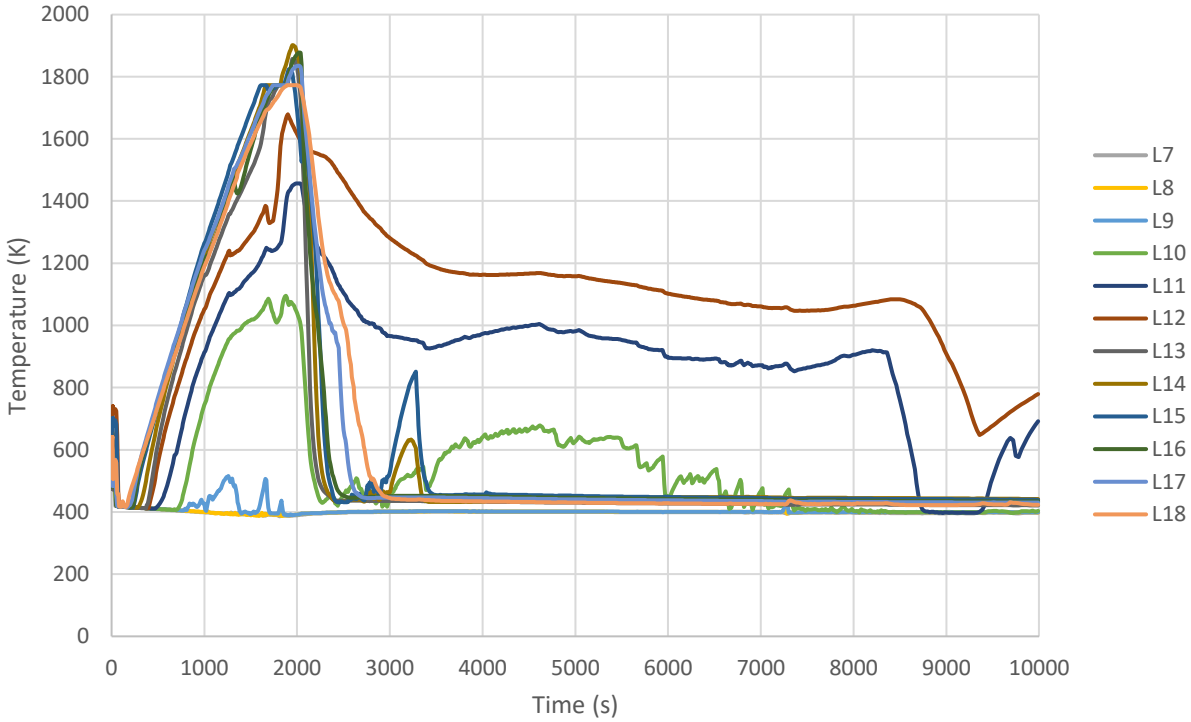

Figure 16: APMT 18m clad temperature in third radial zone.

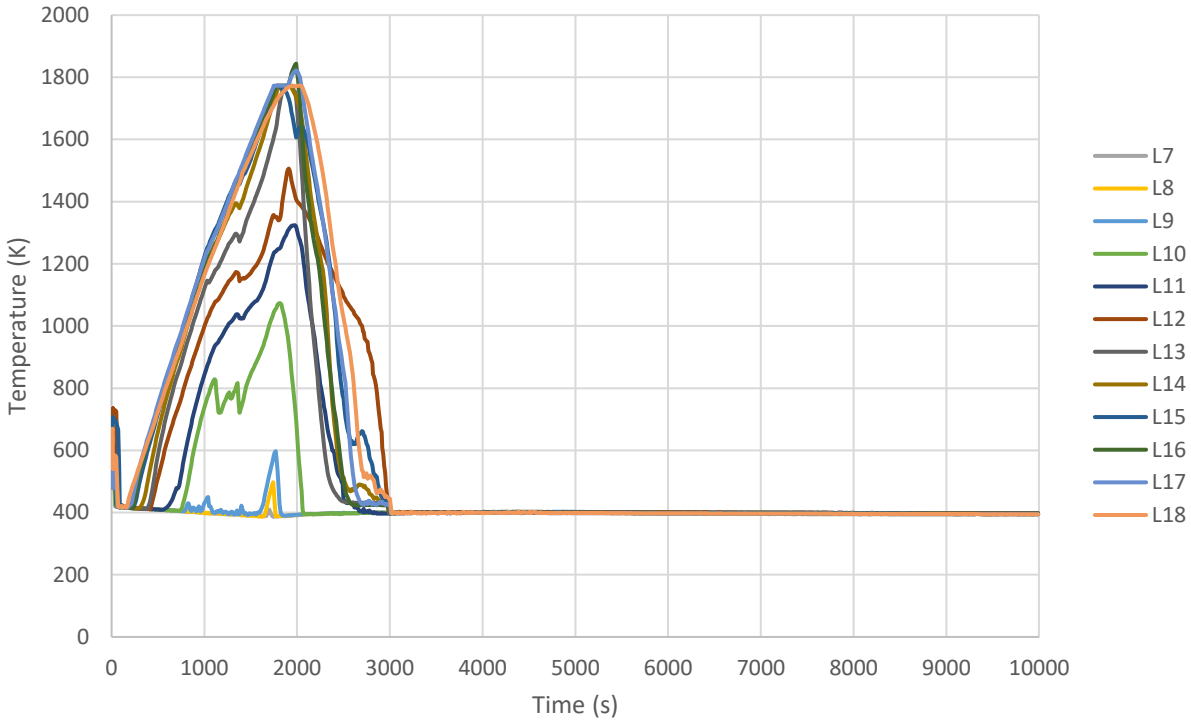

Figure 17: APMT 24m clad temperature in third radial zone.

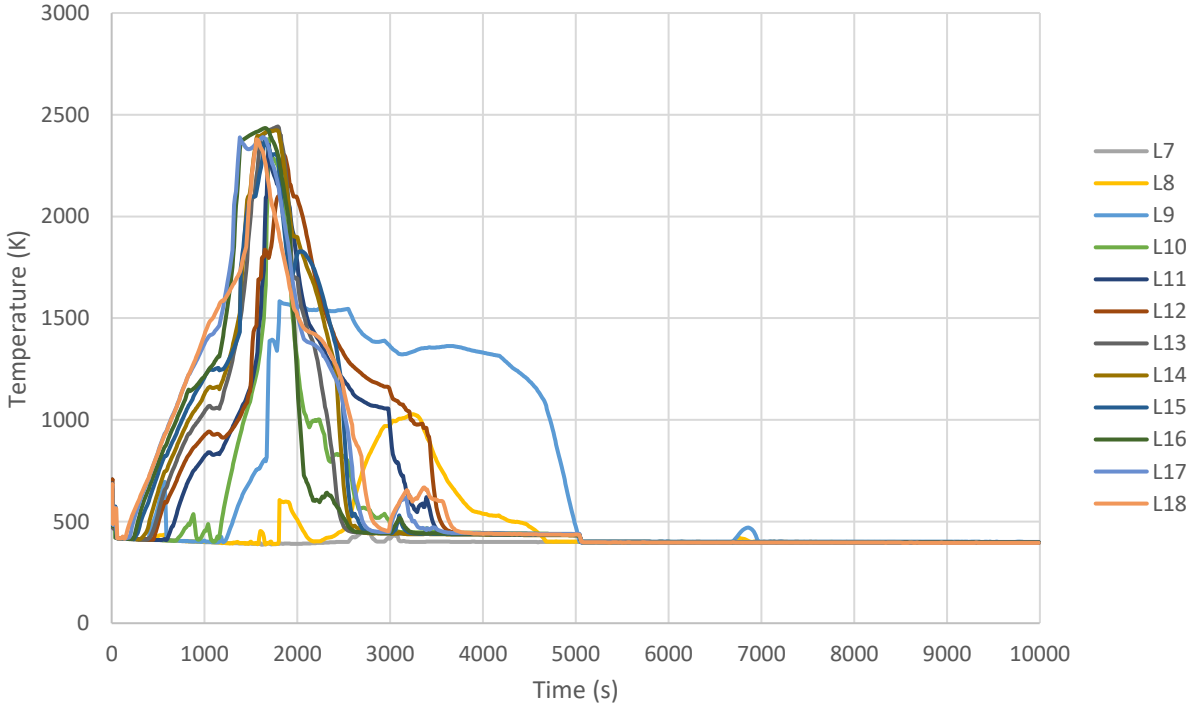

Figure 18: Zry 18m clad temperature in fourth radial zone.

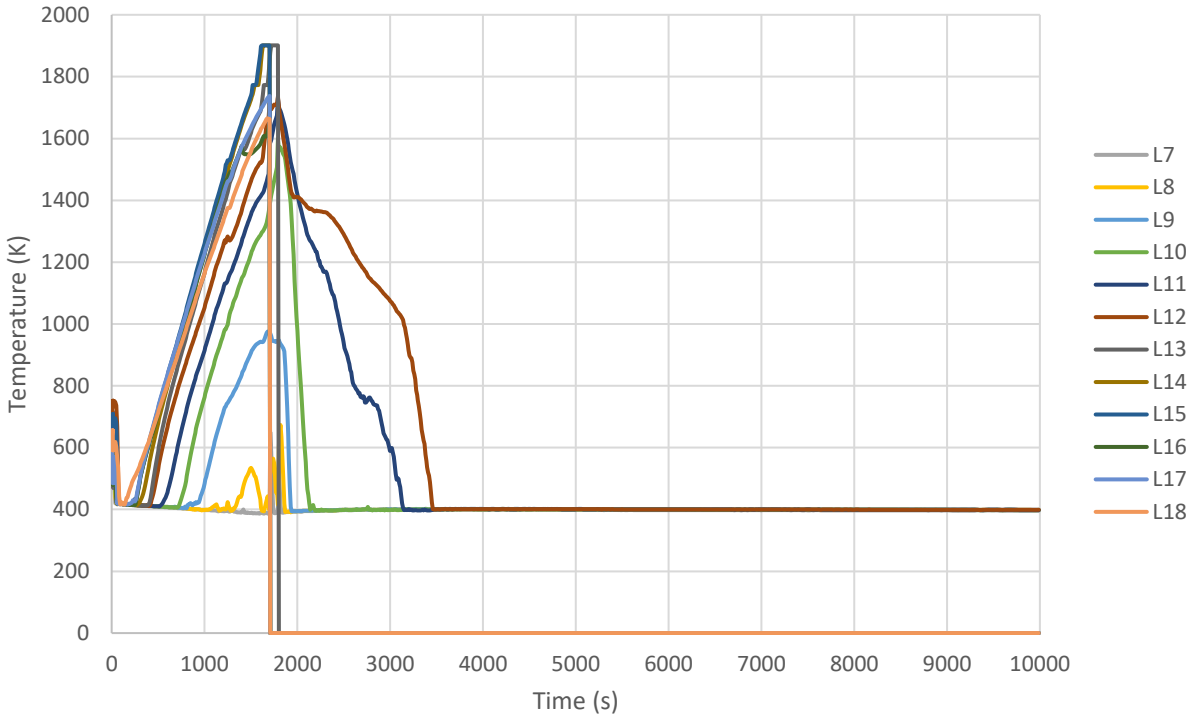

Figure 19: C26M 18m clad temperature in fourth radial zone.

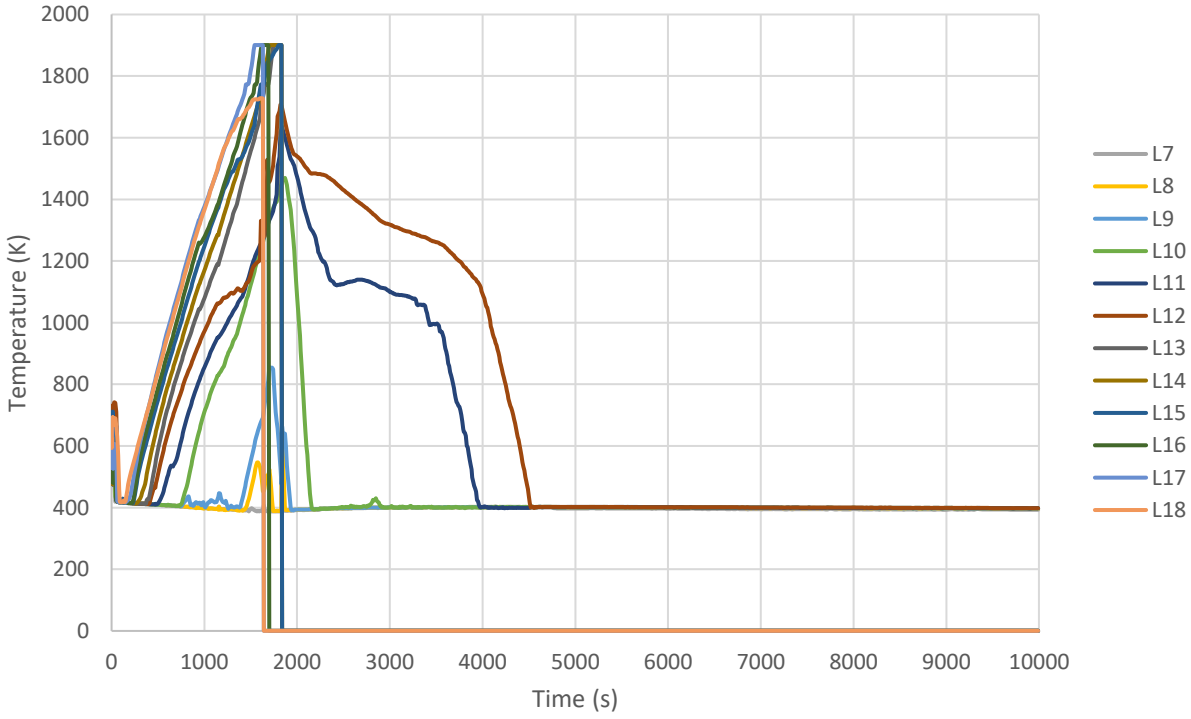

Figure 20: C26M 24m clad temperature in fourth radial zone.

5.2 Hydrogen

The hydrogen produced as calculated by MELCOR for the different cases is shown in Figure 21.

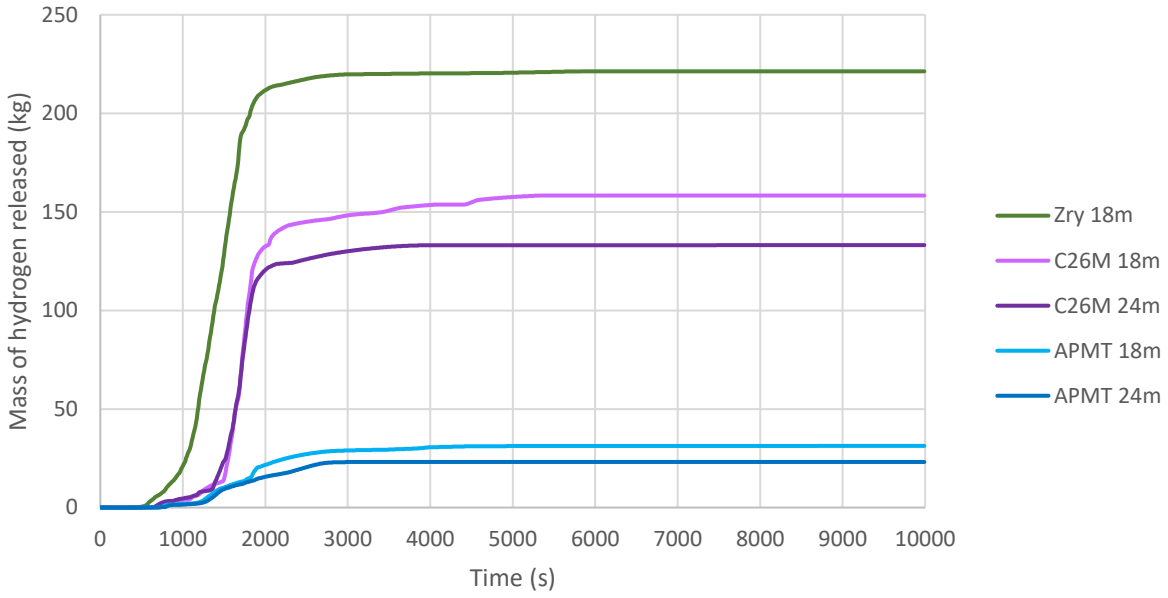

Figure 21: Hydrogen release results for MELCOR calculation cases.

All cases exhibit the expected behavior, beginning to release hydrogen as the LOCA progresses and the fuel is uncovered, before reaching a maximum and ending hydrogen production when the LOCA is recovered and the core is re-submerged by the coolant. Hydrogen production begins earlier for Zry clad than for FeCrAl clad and produces significantly more hydrogen, which is due its less favorable oxidation kinetics. These Zry oxidations release more heat and produce more hydrogen than FeCrAl oxidation, resulting in faster uncovering of the core and an earlier onset of fuel melting in the LOCA.

The APMT FeCrAl cases exhibit relatively low hydrogen production. However, the C26M cases have significantly higher production than APMT. This may be attributed to the lower breakaway oxidation temperature of C26M, which results in the protective Al_2O_3 scale failing earlier and more rapid hydrogen-producing oxidation reactions occurring shortly before the fuel is re-submerged. However, the hydrogen production by C26M starts later and is nonetheless significantly lower than Zry with the 18-month fuel cycle, even with the breakaway oxidation effects.

Moving from the 18-month cycle to the 24-month cycle is not observed to increase the hydrogen release. This is expected as the change in burnup does not substantially alter the decay heat. Indeed, here we see slightly higher hydrogen production (and core melt) with the 18-month cycle. This is likely driven by slight differences in the core power distribution along with the inherent sensitivity of beyond design basis accident calculations to initial conditions. I.e., from this it should not be inferred that *in general* the hydrogen release would be lower with a 24-month cycle

Again, these results indicate sensitivity to the LPSI reactivation time. A later reactivation could lead to the delay in oxidation afforded by FeCrAl being nullified by the later onset of core melt, while an earlier reactivation time (e.g., ~1200s) could prevent the breakaway oxidation behavior in FeCrAl; even earlier (e.g., <1000s) would lead to significantly lower hydrogen generation for both FeCrAl and Zry.

5.3 Fission product release

The total mass of fission products produced as calculated by MELCOR is shown in Figure 22 for the different cases. As expected, the Zry clad case produces a larger total amount of fission products than the FeCrAl C26M clad case for fuel from an 18-month cycle. Both FeCrAl clad cases with HBU fuel also produce less total fission product mass than fuel with Zry clad. The results for the FeCrAl HBU C26M and APMT cases are reasonably close to each other.

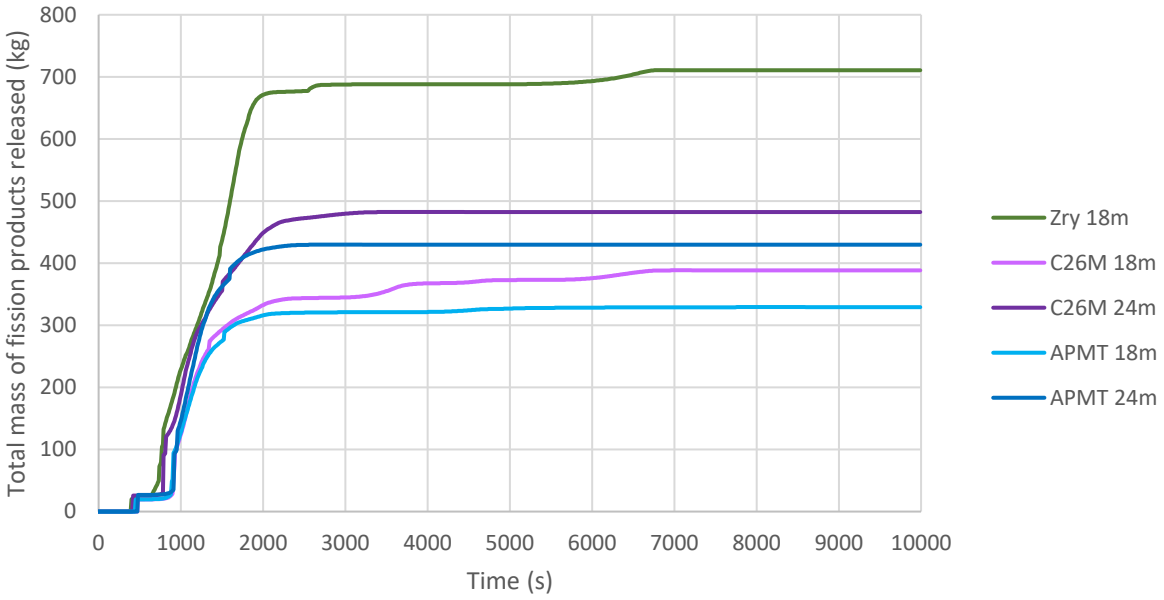

Figure 22: Total fission product release results for MELCOR calculation cases.

The fission product release with the 24-month cycle is appreciably higher than that with the 18-month cycle despite the core melting being lower in this case. This naturally follows from the higher burnup and hence higher fission product inventory in the core. Here, the EOEC average burnup is 35% higher for the 24-month core than the 18-month core. The released mass of fission products is 25% and 30% higher for the C26M and APMT cases respectively, broadly consistent with increase in discharge burnup.

For ATFs to be combined with HBU fuel, it may be desired to demonstrate an overall reduction (or lack of increase) in source term with respect to a Zry reference case. The next step in such an analysis is to propagate the fission product release to an accident consequence analysis. In the U.S., 10CFR50.67 states that when evaluating "proposed design basis changes with respect to potential reactor accidents of exceedingly low probability of occurrence and low risk of public exposure to radiation" a reference value of 0.25 Sv Total Effective Dose Equivalent (TEDE) may be used for an "individual located at any point on the boundary of the exclusion area [10 miles] for any 2-hour period following the onset of the postulated fission product release". [86] Therefore, the TEDE between the scenarios investigated here could be compared. To first order, the reduction in fission product release for the FeCrAl 24-month case compared to the Zry 18-month case will propagate to a reduction in TEDE (although noting that the relative composition of the fission products is different) and thus providing some evidence that a HBU 24-month core could be accommodated.

To demonstrate such a reduction with FeCrAl, the beneficial effect of the alternative clad material must outweigh the increase in potential release caused by higher core fission product inventory. For FeCrAl, the beneficial effect in beyond design basis accident scenarios is an increase in the time taken for the core to melt. For the recovered LOCA scenario investigated here, the extra coping time afforded by the FeCrAl is of the same magnitude as the transient time, specifically the recovery time of the LPSI and this reduced the core melt sufficiently to reduce the overall fission product release of the FeCrAl 24-month cases compared to the Zry reference case despite their higher fission product inventory.

However, it is important to emphasize that a suite of transients must be evaluated, weighted by their relative probabilities, in order to derive the overall source term. In other transients, the additional coping time afforded by FeCrAl may be insufficient to prevent widespread core melt (e.g., an

unrecovered LBLOCA). In such cases, the fission product release from a HBU 24-month core would likely be higher than that from the reference 18-month core, even with FeCrAl cladding.

The individual fission product releases for the five largest MELCOR DCH/RN class contributors are shown in Figure 23 for the 18m C26M case and the relative breakdown is similar for the other cases. The classes of fission products released are broadly the same for both Zry and FeCrAl C26M as the fuel composition and operating conditions are very similar between cases. The dominant fission product classes are XE, CSM and CS. The HBU cases show increased total and class fission product release but retain the same broad class distribution as for the 18-month cases.

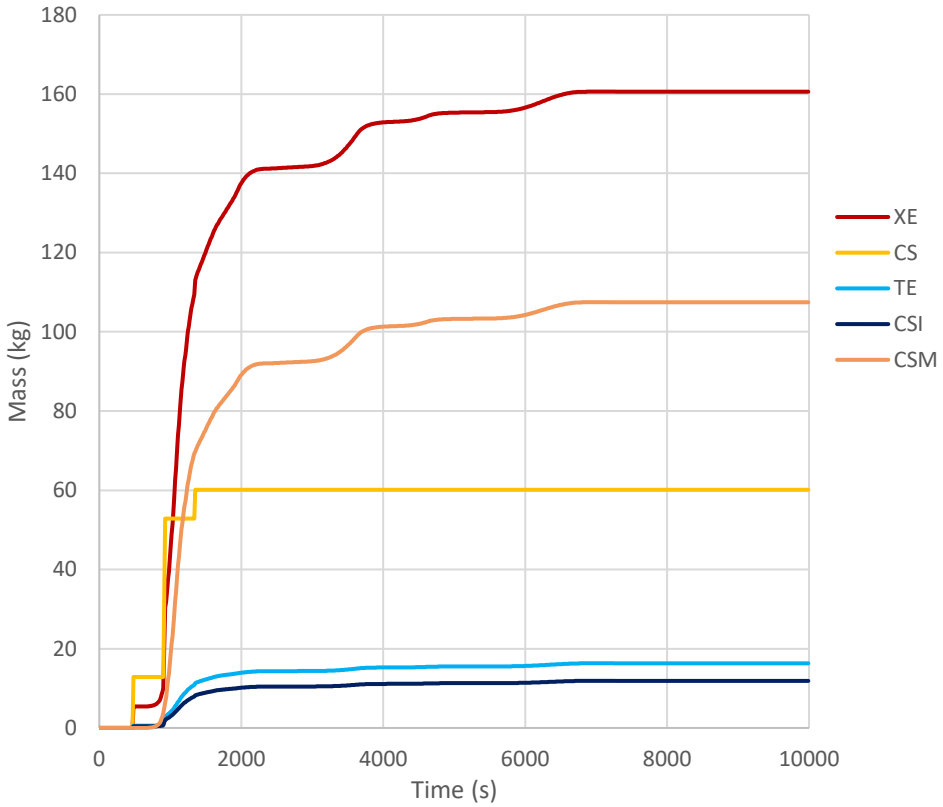

Figure 23: C26M 18m fission product release results.

A potential next step is therefore to utilize the fission product release inventories calculated by MELCOR in a consequence analysis in MACCS. This can be used to determine if the dose at the boundary of the exclusion area has indeed been reduced. The methodology utilized here enables a consistent calculation of the fission products released from MELCOR to be input into MACCS, therefore allowing the increased fission product inventory from a high burnup core (along with the detailed differences in the isotopic breakdown) to be propagated through to the MACCS calculation. This will be performed in future work.

6 Conclusion

A model for FeCrAl clad has been developed within the latest version of MELCOR using the UDM methodology. Overall, the results presented in the previous section show a noticeable improvement in key parameters from the use of FeCrAl C26M compared to Zry as fuel clad. The different material properties and enhanced oxidation resistance of FeCrAl enables a slower rate of core damage and fuel melting, as well as reducing the total amounts of hydrogen produced and fission products released. For the recovered LBLOCA scenario evaluated here, this resulted in a lower overall release, as the additional coping down melting was of the same order as the timeframe for ECCS reactivation.

A case with HBU fuel with FeCrAl clad is also examined to demonstrate quantification of whether the benefits of FeCrAl are outweighed by the increased fission product inventory with HBU fuel. Although the HBU cases

do not show as large an improvement as the normal 18-month fuel cycle cases, the results still improve on the standard Zry clad for the case analyzed for both fission product release and hydrogen production. Further work could analyze a wider range of accident scenarios to determine if the overall source term for a HBU core with FeCrAl clad is lower than that of a typical core with Zry clad. It is noted that in other scenarios, the additional coping time may be of reduced benefit, and hence the increased fission product inventory from HBU operation may prove greater. Also, the detailed fission product release inventories derived through the MELCOR simulation may be used in a MACCS calculation of accident consequences.

These results provide a useful starting point for analysis of FeCrAl clad using the MELCOR UDM methodology, but it should be noted that there is still room to optimize the models. Additionally, future work should include a sensitivity and uncertainty analysis to the parameters of the FeCrAl model. This is particularly important given that for BDBA, the outcome can be highly sensitive to the input parameters, and this appears to be the case for the transient progression in the scenario investigated. The sensitivity to the performance improvement over Zry clad to the ECCS recovery time could also be investigated, to determine if the observed performance benefit is sustained over a wide range of activation times or only holds for very specific circumstances.

Other model improvements could include the use of more detailed data for the FeCrAl C26M alloy. At the time of this work the available data on C26M was limited for those parameters required by MELCOR, necessitating a number of approximations for the material properties. Further experimental analysis on the oxidation behavior in particular may show a need to adjust the simulation approach. More information is also required on possible eutectic interactions in FeCrAl clad, and to investigate whether FeCrAl exhibits the same oxide shell hold-up effects as Zry.

Furthermore, updates to the MELCOR calculation methods may improve the capturing of important interactions. One could be the treatment of oxidation in solid and molten materials. In this work the two FeCrAl alloys, C26M and APMT, are treated identically except for the lower breakaway oxidation temperature defined for C26M. The results presented in the previous section show a marked difference between the FeCrAl cases which may be partly misrepresented due to no oxidation model currently existing in MELCOR for molten materials. As APMT begins experiencing breakaway oxidation at the same temperature as its melting point, 1773 K, MELCOR may be failing to capture the full extent of the oxidation for the APMT cases.

Acknowledgements

We gratefully acknowledge the help of the MELCOR team at SNL, including Jesse Phillips, Troy Haskin, Lucas Albright, and David Luxat; along with Ryan Stewart and SunJong Yoon at INL, and our colleagues Dr Jun Wang, Robert Armstrong, Prof. Michael Corradini and Prof Juliana Pacheco Duarte for their technical advice. This work received funding from the U.S. Department of Energy's (DOE) Light Water Reactor Sustainability (LWRS) Program under subaward from Idaho National Laboratory Prime Contract No. DE-AC07-05ID14517.

References

[1] S. J. Zinkle, K. A. Terrani, J. C. Gehin, L. J. Ott, and L. L. Snead, 'Accident tolerant fuels for LWRs: A perspective', *J. Nucl. Mater.*, vol. 448, no. 1–3, pp. 374–379, 2014.

[2] Y.-H. Koo *et al.*, 'KAERI's development of LWR accident-tolerant fuel', *Nucl. Technol.*, vol. 186, no. 2, pp. 295–304, 2014.

[3] K. Shirvan, 'Implications of accident tolerant fuels on thermal-hydraulic research', *Nucl. Eng. Des.*, vol. 358, p. 110432, Mar. 2020, doi: 10.1016/j.nucengdes.2019.110432.

[4] K. Shirvan and A. Csontos, 'Achieving Sizable Power-Uprate for Existing Fleet Through LEU+ and ATF'. OSF Preprints, Aug. 08, 2022. doi: 10.31219/osf.io/ykxh4.

[5] R. B. Rebak, 'Alloy selection for accident tolerant fuel cladding in commercial light water reactors', *Metall. Mater. Trans. E*, vol. 2, pp. 197–207, 2015.

[6] L. J. Ott, K. R. Robb, and D. Wang, 'Preliminary assessment of accident-tolerant fuels on LWR performance during normal operation and under DB and BDB accident conditions', *J. Nucl. Mater.*, vol. 448, no. 1, pp. 520–533, May 2014, doi: 10.1016/j.jnucmat.2013.09.052.

[7] L. Hallstadius, S. Johnson, and E. Lahoda, 'Cladding for high performance fuel', *Prog. Nucl. Energy*, vol. 57, pp. 71–76, 2012.

[8] Y. Katoh, L. L. Snead, I. Szlufarska, and W. J. Weber, 'Radiation effects in SiC for nuclear structural applications', *Curr. Opin. Solid State Mater. Sci.*, vol. 16, no. 3, pp. 143–152, 2012.
[9] R. B. Rebak, K. A. Terrani, W. P. Gassmann, J. B. Williams, and K. L. Ledford, 'Improving Nuclear Power Plant Safety with FeCrAl Alloy Fuel Cladding', *MRS Adv.*, vol. 2, no. 21–22, pp. 1217–1224, ed 2017, doi: 10.1557/adv.2017.5.
[10] K. Sakamoto *et al.*, 'Development of accident tolerant FeCrAl-ODS fuel cladding for BWRs in Japan', *J. Nucl. Mater.*, vol. 557, p. 153276, Dec. 2021, doi: 10.1016/j.jnucmat.2021.153276.
[11] J. D. Hales, S. R. Novascone, B. W. Spencer, R. L. Williamson, G. Pastore, and D. M. Perez, 'Verification of the BISON fuel performance code', *Ann. Nucl. Energy*, vol. 71, pp. 81–90, Sep. 2014, doi: 10.1016/j.anucene.2014.03.027.
[12] B. Qiu and J. Wang, 'Chapter 7 - FRAPCON and FRAPTRAN codes: Fuel rod performance analysis codes under normal and accident conditions', in *Nuclear Power Plant Design and Analysis Codes*, J. Wang, X. Li, C. Allison, and J. Hohorst, Eds., in Woodhead Publishing Series in Energy. , Woodhead Publishing, 2021, pp. 141–159. doi: 10.1016/B978-0-12-818190-4.00007-3.
[13] R. L. Williamson *et al.*, 'Multidimensional multiphysics simulation of nuclear fuel behavior', *J. Nucl. Mater.*, vol. 423, no. 1, pp. 149–163, Apr. 2012, doi: 10.1016/j.jnucmat.2012.01.012.
[14] J. Kim, C. Shin, H. Oh, and H. Kim, 'ODS Cladding Burst test using DIMAT and Transient Analysis with FRAPTRAN-KATF', presented at the Transactions of the Korean Nuclear Society Virtual Autumn Meeting, Virtual, Oct. 2021.
[15] Y. He, K. Shirvan, Y. Wu, and G. Su, 'Integrating a multi-layer deformation model in FRAPTRAN for accident Tolerant fuel analysis', *Ann. Nucl. Energy*, vol. 133, pp. 441–454, Nov. 2019, doi: 10.1016/j.anucene.2019.05.048.
[16] B. Qiu *et al.*, 'A comparative study on preliminary performance evaluation of ATFs under normal and accident conditions with FRAP-ATF code', *Prog. Nucl. Energy*, vol. 105, pp. 51–60, May 2018, doi: 10.1016/j.pnucene.2017.12.010.
[17] P. Aragón, F. Feria, and L. E. Herranz, 'Modelling FeCrAl cladding thermo-mechanical performance. Part II: Comparative analysis with Zircaloy under LOCA conditions', *Prog. Nucl. Energy*, vol. 163, p. 104838, Sep. 2023, doi: 10.1016/j.pnucene.2023.104838.
[18] K. A. Gamble, T. Barani, D. Pizzocri, J. D. Hales, K. A. Terrani, and G. Pastore, 'An investigation of FeCrAl cladding behavior under normal operating and loss of coolant conditions', *J. Nucl. Mater.*, vol. 491, pp. 55–66, Aug. 2017, doi: 10.1016/j.jnucmat.2017.04.039.
[19] S. K. Lee *et al.*, 'BISON validation of FeCrAl cladding mechanical failure during simulated reactivity-initiated accident conditions', *J. Nucl. Mater.*, vol. 564, p. 153676, Jun. 2022, doi: 10.1016/j.jnucmat.2022.153676.
[20] R. Sweet, P. Mouche, S. Bell, K. Kane, and N. Capps, 'Chromium-coated cladding analysis under simulated LOCA burst conditions', *Ann. Nucl. Energy*, vol. 176, p. 109275, Oct. 2022, doi: 10.1016/j.anucene.2022.109275.
[21] M. Wagih, B. Spencer, J. Hales, and K. Shirvan, 'Fuel performance of chromium-coated zirconium alloy and silicon carbide accident tolerant fuel claddings', *Ann. Nucl. Energy*, vol. 120, pp. 304–318, Oct. 2018, doi: 10.1016/j.anucene.2018.06.001.
[22] R. L. Williamson *et al.*, 'BISON: A Flexible Code for Advanced Simulation of the Performance of Multiple Nuclear Fuel Forms', *Nucl. Technol.*, vol. 207, no. 7, pp. 954–980, Jul. 2021, doi: 10.1080/00295450.2020.1836940.
[23] R. C. Martineau, 'The MOOSE Multiphysics Computational Framework for Nuclear Power Applications: A Special Issue of Nuclear Technology', *Nucl. Technol.*, vol. 207, no. 7, pp. iii–viii, Jul. 2021, doi: 10.1080/00295450.2021.1915487.
[24] C. J. Permann *et al.*, 'MOOSE: Enabling massively parallel multiphysics simulation', *SoftwareX*, vol. 11, p. 100430, Jan. 2020, doi: 10.1016/j.softx.2020.100430.
[25] L. L. Humphries *et al.*, 'MELCOR Computer Code Manuals Volume 1: Primer and Users' Guide', Sandia National Lab, Albuquerque, NM, 2.2.19018, Jan. 2021. doi: 10.2172/1433069.

[26] L. L. Humphries *et al.*, 'MELCOR Computer Code Manuals Volume 2: Reference Manual', Sandia National Lab, Albuquerque, NM, 2.2.18019, Jan. 2021. doi: 10.2172/1433069.
[27] H. N. Jow, J. L. Sprung, L. T. Ritchie, J. A. Rollstin, and D. I. Chanin, 'MELCOR Accident Consequence Code System (MACCS)', Nuclear Regulatory Commission, Washington, DC (USA). Div. of Systems Research; Sandia National Lab. (SNL-NM), Albuquerque, NM (United States), NUREG/CR-4691-Vol.2; SAND-86-1562-Vol.2, Feb. 1990. doi: 10.2172/7247757.
[28] K. Robb, J. McMurray, and K. Terrani, 'Severe accident analysis of BWR core fueled with UO2/FeCrAl with updated materials and melt properties from experiments', *ORNL TM-2016237 Oak Ridge TN*, vol. 10, p. 1259432, 2016.
[29] J. Wang, M. Mccabe, T. Christopher Haskin, Y. Wu, G. Su, and M. L. Corradini, 'Iron–Chromium–Aluminum (FeCrAl) Cladding Oxidation Kinetics and Auxiliary Feedwater Sensitivity Analysis—Short-Term Station Blackout Simulation of Surry Nuclear Power Plant', *J. Nucl. Eng. Radiat. Sci.*, vol. 4, no. 4, Sep. 2018, doi: 10.1115/1.4040887.
[30] J. Wang, H. J. Jo, and M. L. Corradini, 'Potential Recovery Actions from a Severe Accident in a PWR: MELCOR Analysis of a Station Blackout Scenario', *Nucl. Technol.*, vol. 204, no. 1, pp. 1–14, Oct. 2018, doi: 10.1080/00295450.2018.1464838.
[31] J. Wang *et al.*, 'Accident tolerant clad material modeling by MELCOR: Benchmark for SURRY Short Term Station Black Out', *Nucl. Eng. Des.*, vol. 313, pp. 458–469, Mar. 2017, doi: 10.1016/j.nucengdes.2017.01.002.
[32] B. J. Merrill and S. M. Bragg-Sitton, 'Status report of advanced cladding modeling work to assess cladding performance under accident conditions', Idaho National Lab.(INL), Idaho Falls, ID (United States), 2013.
[33] B. J. Merrill, S. M. Bragg-Sitton, and P. W. Humrickhouse, 'Modification of MELCOR for severe accident analysis of candidate accident tolerant cladding materials', *Nucl. Eng. Des.*, vol. 315, pp. 170–178, Apr. 2017, doi: 10.1016/j.nucengdes.2017.02.021.
[34] P. W. Humrickhouse and B. J. Merrill, 'Status Report on Modifications to MELCOR for Modeling of Accident Tolerant Fuel (ATF)', Idaho National Lab.(INL), Idaho Falls, ID (United States), 2017.
[35] T. Feng *et al.*, 'Quantification of the effect of Cr-coated-Zircaloy cladding during a short term station black out', *Nucl. Eng. Des.*, vol. 363, p. 110678, Jul. 2020, doi: 10.1016/j.nucengdes.2020.110678.
[36] Z. Guo *et al.*, 'Uncertainty analysis of ATF Cr-coated-Zircaloy on BWR in-vessel accident progression during a station blackout', *Reliab. Eng. Syst. Saf.*, vol. 213, p. 107770, Sep. 2021, doi: 10.1016/j.ress.2021.107770.
[37] Z. Guo, R. Dailey, Y. Zhou, Z. Sun, J. Wang, and M. L. Corradini, 'Effect of ATF Cr-coated-Zircaloy on BWR In-vessel Accident Progression during a Station Blackout', *Nucl. Eng. Des.*, vol. 372, p. 110979, Feb. 2021, doi: 10.1016/j.nucengdes.2020.110979.
[38] J. Wang, R. Dailey, Z. Guo, Y. Zhou, P. Humrickhouse, and M. L. Corradini, 'Accident tolerant fuels (FeCrAl Cladding & Coating) performance analysis in Boiling Water Reactor (BWR) by the MELCOR 1.8.6 UDGC', *Nucl. Eng. Des.*, vol. 371, p. 110974, Jan. 2021, doi: 10.1016/j.nucengdes.2020.110974.
[39] L. Humphries, B. Beeny, T. Haskin, L. Albright, and F. Gelbard, 'MELCOR Code Change History: Revision 18019 to 21402', Sandia National Lab. (SNL-NM), Albuquerque, NM (United States), SAND2022-0114, Dec. 2021. doi: 10.2172/1855048.
[40] L. L. Humphries, J. L. Phillips, R. C. Schmidt, B. A. Beeny, D. L. Louie, and N. E. Bixler, 'MELCOR Code Change History: Revision 14959 to 18019', Sandia National Laboratory, Sandia National Laboratory, SAND2020-14302, Dec. 2020.
[41] C. Faucett, B. Beeny, and K. Vierow Kirkland, 'MELCOR Modeling of Combined Accident Tolerant Fuel and Reactor Core Isolation Cooling System Operation', presented at the 2020 International Conference on Nuclear Engineering collocated with the ASME 2020 Power Conference, American Society of Mechanical Engineers Digital Collection, Oct. 2020. doi: 10.1115/ICONE2020-16409.

[42] P. Mičian, ‘Investigation of the hydrogen production by the FeCrAl nuclear fuel cladding using MELCOR 2.2’, presented at the Electrical Engineering, Information and Communication Technologies 2022, Brno, Czech Republic, Apr. 2022. doi: 10.13164/eeict.2022.220.
[43] A. G. Le Coq, R. C. Martin, and K. D. Linton, ‘Transportation Planning for Irradiated Fuel-Cladding and Integral FeCrAl Experiments’, ORNL/TM--2019/1123, 1506785, Feb. 2019. doi: 10.2172/1506785.
[44] R. B. Rebak, V. K. Gupta, and M. Larsen, ‘Oxidation Characteristics of Two FeCrAl Alloys in Air and Steam from 800°C to 1300°C’, *JOM*, vol. 70, no. 8, pp. 1484–1492, Aug. 2018, doi: 10.1007/s11837-018-2979-9.
[45] Y. Yamamoto, K. Kane, B. A. Pint, A. Trofimov, and H. Wang, ‘Report on exploration of new FeCrAl heat variants with improved properties’, Oak Ridge National Lab.(ORNL), Oak Ridge, TN (United States), 2019.
[46] Y. Yamamoto, B. A. Pint, K. A. Terrani, K. G. Field, Y. Yang, and L. L. Snead, ‘Development and property evaluation of nuclear grade wrought FeCrAl fuel cladding for light water reactors’, *J. Nucl. Mater.*, vol. 467, pp. 703–716, Dec. 2015, doi: 10.1016/j.jnucmat.2015.10.019.
[47] Kanthal, ‘Kanthal APMT Construction Materials’, Datasheet, Dec. 2021.
[48] R. B. Rebak, ‘Development of LWR fuels with enhanced accident tolerance. Final report’, General Electric Global Research Center, Schenectady, NY (United States), DOE-NE0008221, Dec. 2018. doi: 10.2172/1488931.
[49] K. A. Terrani *et al.*, ‘Uniform corrosion of FeCrAl alloys in LWR coolant environments’, *J. Nucl. Mater.*, vol. 479, pp. 36–47, Oct. 2016, doi: 10.1016/j.jnucmat.2016.06.047.
[50] B. A. Pint, K. A. Terrani, M. P. Brady, T. Cheng, and J. R. Keiser, ‘High temperature oxidation of fuel cladding candidate materials in steam–hydrogen environments’, *J. Nucl. Mater.*, vol. 440, no. 1, pp. 420–427, Sep. 2013, doi: 10.1016/j.jnucmat.2013.05.047.
[51] B. A. Pint, ‘Performance of FeCrAl for accident-tolerant fuel cladding in high-temperature steam’, *Corros. Rev.*, vol. 35, no. 3, pp. 167–175, 2017.
[52] B. A. Pint, K. A. Terrani, and R. B. Rebak, ‘Steam Oxidation Behavior of FeCrAl Cladding’, in *Proceedings of the 18th International Conference on Environmental Degradation of Materials in Nuclear Power Systems – Water Reactors*, J. H. Jackson, D. Paraventi, and M. Wright, Eds., in The Minerals, Metals & Materials Series. Cham: Springer International Publishing, 2019, pp. 1451–1460. doi: 10.1007/978-3-030-04639-2_96.
[53] B. A. Pint, K. A. Terrani, Y. Yamamoto, and L. L. Snead, ‘Material Selection for Accident Tolerant Fuel Cladding’, *Metall. Mater. Trans. E*, vol. 2, no. 3, pp. 190–196, Sep. 2015, doi: 10.1007/s40553-015-0056-7.
[54] X. Wu, T. Kozlowski, and J. D. Hales, ‘Neutronics and fuel performance evaluation of accident tolerant FeCrAl cladding under normal operation conditions’, *Ann. Nucl. Energy*, vol. 85, pp. 763–775, Nov. 2015, doi: 10.1016/j.anucene.2015.06.032.
[55] R. O. Gauntt *et al.*, ‘MELCOR Computer Code Manuals Volume 3: Demonstration Problems Version 2.0’, Sandia National Laboratory, Sandia National Laboratory, Unpublished draft NUREG/CR-6119; SAND2008-xxxx; Vol. 3, Rev. 1, Sep. 2008.
[56] R. O. Gauntt *et al.*, ‘MELCOR Computer Code Manuals Volume 3: Demonstration Problems Version 1.8.5’, Sandia National Laboratory, Sandia National Laboratory, NUREG/CR-6119; SAND2001-0929P; Vol. 3, Rev. 0, May 2001.
[57] M. M. Pilch, ‘Evaluation of Radiological Consequences of Design Basis Accidents At Operating Reactors Using The Revised Source Term’, U.S. Nuclear Regulatory Commission, Sandia National Laboratory, Letter Report for Office of Nuclear Regulatory Research, Sep. 1998.
[58] L. Soffer, S. B. Burson, C. M. Ferrell, R. Y. Lee, and J. N. Ridgely, ‘Accident source terms for Light-Water Nuclear Power Plants Final report’, United States, 1995.
[59] ANS Standards Committee, ‘Decay heat power in light water reactors’, Technical Report ANSI/ANS-5.1-1994, American Nuclear Society, USA, 1993.
[60] Kanthal, ‘Kanthal APMT Construction Materials’, Datasheet, Feb. 2021.

[61] K. G. Field, M. A. Snead, Y. Yamamoto, and K. A. Terrani, ‘Handbook on the Material Properties of FeCrAl Alloys for Nuclear Power Production Applications’, ORNL/SPR-2018/905, Aug. 2018. doi: 10.2172/1474581.
[62] K. G. Field, M. A. Snead, Y. Yamamoto, and K. A. Terrani, ‘Handbook on the Material Properties of FeCrAl Alloys for Nuclear Power Production Applications’, ORNL/TM-2017-186, Aug. 2017.
[63] K. R. Robb, ‘Analysis of the FeCrAl Accident Tolerant Fuel Concept Benefits during BWR Station Blackout Accidents’, Oak Ridge National Lab. (ORNL), Oak Ridge, TN (United States), Jan. 2015. Accessed: Jun. 28, 2022. [Online]. Available: https://www.osti.gov/biblio/1213328
[64] Y. Yamamoto, M. A. Snead, K. G. Field, and K. A. Terrani, ‘Handbook of the Materials Properties of FeCrAl Alloys For Nuclear Power Production Applications’, Oak Ridge National Lab. (ORNL), Oak Ridge, TN (United States), ORNL/TM-2017/186, Aug. 2017. doi: 10.2172/1400207.
[65] K. R. Robb, M. Howell, and L. J. Ott, ‘Parametric and Experimentally Informed BWR Severe Accident Analysis Using FeCrAl’, Oak Ridge National Lab. (ORNL), Oak Ridge, TN, ORNL/SPR-2017/373, Aug. 2017.
[66] M. W. Chase, ‘NIST-JANAF Thermochemical Tables, Fourth Edition’, *J. Phys. Chem. Ref. Data*, vol. 9, pp. 1–1951, 1998.
[67] P. W. Humrickhouse and B. J. Merrill, ‘Modifications to MELCOR 1.8. 6 for modeling Accident Tolerant Fuel in Boiling Water Reactors’, Idaho National Lab.(INL), Idaho Falls, ID (United States), 2018.
[68] ‘Review of Accident Tolerant Fuel Concepts with Implications to Severe Accident Progression and Radio’, NRC Web. Accessed: Feb. 14, 2024. [Online]. Available: https://www.nrc.gov/reading-rm/doc-collections/nuregs/contract/cr7282/index.html
[69] H. Ebrahimgol, M. Aghaie, and A. Zolfaghari, ‘Evaluation of ATFs in core degradation of a PWR in unmitigated SBLOCA’, *Ann. Nucl. Energy*, vol. 152, p. 107961, Mar. 2021, doi: 10.1016/j.anucene.2020.107961.
[70] L. Yin *et al.*, ‘Uniform corrosion of FeCrAl cladding tubing for accident tolerant fuels in light water reactors’, *J. Nucl. Mater.*, vol. 554, p. 153090, Oct. 2021, doi: 10.1016/j.jnucmat.2021.153090.
[71] S. Dryepondt, K. A. Unocic, D. T. Hoelzer, C. P. Massey, and B. A. Pint, ‘Development of low-Cr ODS FeCrAl alloys for accident-tolerant fuel cladding’, *J. Nucl. Mater.*, vol. 501, pp. 59–71, Apr. 2018, doi: 10.1016/j.jnucmat.2017.12.035.
[72] C. Goodson and K. Geelhood, ‘Degradation and Failure Phenomena of Accident Tolerant Fuel Concepts: FeCrAl Alloy Cladding’, Pacific Northwest National Laboratory, PNNL-30445, Sep. 2020.
[73] C. Kim, C. Tang, M. Grosse, Y. Maeng, C. Jang, and M. Steinbrueck, ‘Oxidation mechanism and kinetics of nuclear-grade FeCrAl alloys in the temperature range of 500–1500 °C in steam’, *J. Nucl. Mater.*, vol. 564, p. 153696, Jun. 2022, doi: 10.1016/j.jnucmat.2022.153696.
[74] C. P. Massey, K. A. Terrani, S. N. Dryepondt, and B. A. Pint, ‘Cladding burst behavior of Fe-based alloys under LOCA’, *J. Nucl. Mater.*, vol. 470, pp. 128–138, Mar. 2016, doi: 10.1016/j.jnucmat.2015.12.018.
[75] S. B. Bell, K. A. Kane, C. P. Massey, L. A. Baldesberger, D. Lutz, and B. A. Pint, ‘Strength and rupture geometry of un-irradiated C26M FeCrAl under LOCA burst testing conditions’, *J. Nucl. Mater.*, vol. 557, p. 153242, Dec. 2021, doi: 10.1016/j.jnucmat.2021.153242.
[76] S. Ghosh, ‘State-of-the-Art Reactor Consequence Analyses (SOARCA) Project Sequoyah Integrated Deterministic and Uncertainty Analyses’, USNRC, Sandia National Laboratory, NUREG/CR-7245, Oct. 2019.
[77] M. Barrachin, D. Gavillet, R. Dubourg, and A. De Bremaecker, ‘Fuel and fission product behaviour in early phases of a severe accident. Part I: Experimental results of the PHEBUS FPT2 test’, *J. Nucl. Mater.*, vol. 453, no. 1–3, pp. 340–354, 2014.

[78] K. R. Robb, J. W. McMurray, and K. A. Terrani, ‘M2FT-16OR020205042: Severe Accident Analysis Of BWR Core Fueled With UO2/FeCrAl with Updated Materials and Melt Properties From Experiments’, Oak Ridge National Lab. (ORNL), Oak Ridge, TN (United States), ORNL/TM-2016/237, Jun. 2016. doi: 10.2172/1259432.
[79] K. Ogujiuba, K. H. N. Nguyen, Choi Y. J., and J. Hou, ‘Neutronics Assessment of Advanced Fuel Claddings in the Equilibrium LWR Core Design’, in *Transactions of the American Nuclear Society*, Phoenix, AZ, Nov. 2022, pp. 569–572.
[80] J. A. Turner *et al.*, ‘The Virtual Environment for Reactor Applications (VERA): Design and architecture’, *J. Comput. Phys.*, vol. 326, pp. 544–568, Dec. 2016, doi: 10.1016/j.jcp.2016.09.003.
[81] B. T. Rearden and M. A. Jessee, ‘SCALE code system’, Oak Ridge National Lab.(ORNL), Oak Ridge, TN (United States), 2018.
[82] S. M. Bowman, ‘SCALE 6: comprehensive nuclear safety analysis code system’, *Nucl. Technol.*, vol. 174, no. 2, pp. 126–148, 2011.
[83] P. W. Humrickhouse and B. J. Merrill, ‘Status Report on Modifications to MELCOR for modeling of Accident Tolerant Fuel (ATF)’, Idaho National Lab. (INL), Idaho Falls, ID (United States), INL/EXT-17-43162-Rev000, Aug. 2017. doi: 10.2172/1472051.
[84] Jeff Cardoni, ‘Radionuclide Inventory and Decay Heat Quantification Methodology for Severe Accident Simulations’, Sandia National Laboratory, Albuquerque, NM, SANDIA REPORT SAND2014-17667, Sep. 2014.
[85] L. Kmetyk and L. Smith, ‘Summary of MELCOR 1.8.2 calculations for three LOCA sequences (AG, S2D, and S3D) at the Surry Plant’, Nuclear Regulatory Commission, Washington, DC (United States). Div. of Safety Issue Resolution; Sandia National Lab. (SNL-NM), Albuquerque, NM (United States); Geo-Centers, Inc., Albuquerque, NM (United States), NUREG/CR-6107; SAND-93-2042, Mar. 1994. doi: 10.2172/142546.
[86] ‘§ 50.67 Accident source term.’, NRC Web. Accessed: Feb. 23, 2024. [Online]. Available: https://www.nrc.gov/reading-rm/doc-collections/cfr/part050/part050-0067.html